Epigenetic Alteration of Smooth Muscle Cells Regulates Endothelin-Dependent Blood Pressure and Hypertensive Arterial Remodeling

.

Kevin D. Mangum[1]; Qinmengge Li[2]; Katherine Hartmann[3]; Tyler M. Bauer[1]; Sonya J. Wolf [1,2]; James Shadiow[1], Jadie Y. Moon[1,2]; Emily C. Barrett[1]; Amrita D. Joshi[1]; Gabriela Saldana de Jimenez[1]; Zara Ahmed[1]; Rachael Wasikowski[2]; Kylie Boyer[1]; Andrea T. Obi[1,2]; Frank M. Davis[1]; Lin Chang[4]; Lam C. Tsoi[2]; Johann Gudjonsson[2]; Scott M. Damrauer[3], Katherine A. Gallagher[1,2]

[1]Section of Vascular Surgery, Department of Surgery, University of Michigan, Ann Arbor, MI
[2]Department of Microbiology and Immunology, University of Michigan, Ann Arbor, MI
[3]Department of Surgery, University of Pennsylvania, Philadelphia, PA
[4]Department of Internal Medicine, University of Michigan, Ann Arbor, MI

Corresponding Author:
Katherine A. Gallagher, MD
Ira Doan Professor of Surgery
Departments of Surgery and Immunology
University of Michigan
1500 East Medical Center Drive, SPC 5867
Ann Arbor, MI 48109-5867
Phone: (734) 936-5820
Fax: (734) 647-9867
E-mail: kgallag@med.umich.edu

The authors have declared that no conflict of interest exists.

Abstract

Long-standing hypertension (HTN) affects multiple organs and leads to pathologic arterial remodeling, which is driven by smooth muscle cell (SMC) plasticity. To identify relevant genes regulating SMC function in HTN, we considered Genome Wide Association Studies (GWAS) of blood pressure, focusing on genes encoding epigenetic enzymes, which control SMC fate in cardiovascular disease. Using statistical fine mapping of the KDM6 (*JMJD3*) locus, we found that rs62059712 is the most likely casual variant, with each major T allele copy associated with a 0.47 mmHg increase in systolic blood pressure. We show that the T allele decreased *JMJD3* transcription in SMCs via decreased SP1 binding to the *JMJD3* promoter. Using our unique SMC-specific Jmjd3-deficient murine model ($Jmjd3^{flox/flox}Myh11^{CreERT}$), we show that loss of *Jmjd3* in SMCs results in HTN due to decreased *EDNRB* expression and increased *EDNRA* expression. Importantly, the Endothelin Receptor A antagonist, BQ-123, reversed HTN after Jmjd3 deletion *in vivo*. Additionally, single cell RNA-sequencing (scRNA-seq) of human arteries revealed strong correlation between *JMJD3* and *EDNRB* in SMCs. Further, JMJD3 is required for SMC-specific gene expression, and loss of JMJD3 in SMCs increased HTN-induced arterial remodeling. Our findings link a HTN-associated human DNA variant with regulation of SMC plasticity, revealing targets that may be used in personalized management of HTN.

Introduction

Hypertension (HTN) contributes to significant morbidity and mortality in the United States due to its detrimental effects on end-organs including the cardiovascular system (1). Blood pressure (BP) is directly regulated by peripheral vascular resistance (vessel tone), which is mediated by vascular smooth muscle cells (SMCs) (2). Proper BP control requires vascular SMC contraction and relaxation, which is regulated by pharmacologic and mechanical stimuli. Endothelin-1, a potent vasoconstrictor, binds to the endothelin receptor, leading to myosin light chain phosphorylation and SMC contraction. Two endothelin receptors are expressed in SMCs (A and B); however, EDNRA is the predominant receptor mediating SMC contractility and vessel tone (3). In contrast, the effect of EDNRB on SMC function is less established, since recent reports have indicated dual roles for EDNRB (3-5). Endothelin receptor activation mediates SMC contractility and HTN, and endothelin receptor blockade decreases BP in experimental models of HTN (4).

SMC contractility/function is determined by SMC phenotype, which alternates between contractile or synthetic phenotypes, depending on upstream cues. The contractile phenotype is induced by mechanical (e.g., stretch) and molecular (e.g., TGFβ) stimuli, which modulate downstream gene expression via the transcription factors (TFs) serum response factor (SRF), myocardin, and the myocardin-related transcription factors (MRTFs) (6-9). Other TFs such as SP1 and the SMAD family induce genes required for the contractile SMC phenotype (10, 11). In contrast, the synthetic SMC phenotype occurs in atherosclerosis, HTN, and restenosis and is driven by PDGF, inflammatory cytokines, and BMP (12-14). The TFs, KLF4 and ELK1, repress SMC differentiation and promote the synthetic phenotype (15, 16). The precise regulation of SMC differentiation by these upstream cues is highly relevant in cardiovascular disease during which vascular SMCs become phenotypically modulated and contribute to pathology. Specifically, suring disease, SMC genes (*ACTA2, TAGLN, CNN1, MYH11*) are repressed while proliferative-associated genes (*KLF4, FOS*) are increased (13, 17). Epigenetic mechanisms have been

previously shown by our group and others to regulate cell phenotypes and control downstream gene expression in homeostatic and pathologic states (18-20). In particular, epigenetic alteration of chromatin structure by epigenetic enzymes and TFs influences SMC phenotype during development and cardiovascular pathology (21-27).

Genome wide association studies (GWAS) have identified numerous genetic loci associated with cardiovascular diseases including HTN (28). Several GWAS for BP have identified a genome-wide significant association for systolic blood pressure (SBP) at the *JMJD3* (also known as *KDM6B*) locus, which encodes the histone demethylase JMJD3 (29). Notably, JMJD3 is known to play a role in abdominal aortic aneurysm formation and control inflammatory gene expression in innate immune cells in cardiometabolic disease (30, 31).

Here, we use statistical fine mapping to prioritize rs62059712 as the single high-confidence causal signal at the *JMJD3* locus. We use mechanistic studies to link this genetic variant to SBP through changes in *JMJD3* transcription in human and murine SMCs via SP1 TF binding. SMC-specific deletion of *Jmjd3* in mice ($Jmjd3^{flox/flox}Myh11^{CreERT}$) resulted in increased BP in an Angiotensin II model of HTN, which was due to decreased *EDNRB* and increased *EDNRA,* genes encoding expression of Endothelin Receptors A and B, respectively, in SMCs. Endothelin receptor antagonism eliminated increased vessel contractility after JMJD3 deletion *ex vivo* and *in vivo*. Additionally, JMJD3 loss in SMCs enhanced endothelin-ERK activation, resulting in increased SMC phenotypic modulation after vascular injury (i.e. chronic hypertension). Our study provides a mechanistic link between human genetic variation, *JMJD3* expression in SMCs associated with BP alterations, and an SMC phenotypic switch in a murine model, and also identifies a genetic target that may be used to develop previously unknown anti-HTN therapies.

Results

rs62059712 minor C allele increases JMJD3 transcription via enhanced SP1 binding to a regulatory region in the JMJD3 promoter

During cardiovascular diseases (e.g., atherosclerosis) SMCs lose their mature, contractile markers, and switch to a synthetic, proliferative phenotype (13). There remains a knowledge gap in the specific downstream mechanisms that underlie SMC plasticity. Our group and others have identified that epigenetic pathways regulate cell plasticity in cardiovascular disease (27, 32). To identify translationally relevant epigenetic mechanisms regulating BP, we analyzed large GWAS for BP to identify human variants located within or near genes encoding various chromatin modifying enzymes (CMEs) with previously identified roles in cardiovascular disease (29, 33, 34). Our most promising target was the genome-wide association between the *KDM6B* (*JMJD3)* locus and SBP. *JMJD3* encodes a histone demethylase that regulates macrophage phenotype in cardiometabolic diseases (30, 31, 35). The major allele (T) of the lead variant rs62059712 is associated with increased SBP (0.47 mmHg increase; CI 0.28-0.56). A phenome wide association analysis in OpenGWAS and the GWAS Catalog identified association of rs62059712 with other related phenotypes including diastolic blood pressure, pulse pressure, and use of antihypertensive agents including those acting on the renin-angiotensin system, calcium channel blockers, and diuretics **(Supplementary Table 1).**

To refine the signal at the *JMJD3* locus and prioritize potential causal variants, we performed statistical fine mapping using Bayes factor analysis. We considered a 500kb locus, 250kb upstream and downstream of rs62059712. Our analysis identified the lead variant, rs62059712, as the single high-confidence causal signal at this locus (posterior inclusion probability of 0.98, **Table 1**), providing strong supportive evidence for this variant. In addition to the candidate variant, we also considered the effect of SNPs in high LD. Using HaploReg we identified an additional variant, rs74480102, approximately 2.4KB downstream of rs62059712 in strong LD with rs62059712 (defined in this study as r^2>0.3 and D' 1).

To locate rs62059712 and rs74480102 in relation to the *JMJD3* gene and possible alignment with features of open chromatin, we utilized the publicly accessible UCSC Genome Browser (36). Notably, rs62059712 and rs74480102 were both located upstream of the *JMJD3* gene within regions that aligned with several features of active transcription including H3K27 acetylation ChIP-seq peaks, DNase Hypersensitive Sites (DHS), and vertebral conservation **(Figure 1A)**. Thus, we hypothesized that rs62059712 (within DHS1) and/or rs74480102 (within DHS2) altered *JMJD3* transcription by influencing chromatin and TF accessibility to one or both regions. Since SMC contractility directly regulates vascular tone, and thus BP, and because our phenome-wide analysis linked rs62059712 genotype to anti-hypertensive agents that act on SMCs, we hypothesized that *JMJD3* expression in SMCs was important for BP regulation. To test this, we generated an allelic series of luciferase reporter constructs corresponding to major and minor alleles for both SNPs, transfected each into human SMCs (HuSMCs), and measured luciferase activity. The rs62059712 minor C allele demonstrated increased transcriptional activity compared to the major T allele in HuSMCs and mAoSMCs **(Figure 1B-C, Supplemental Figure 1 A-B)**. Notably, there was no difference in luciferase activity between the rs74480102 major G and minor A alleles **(Figure 1C)**. Importantly, rs62059712 did not exhibit allele-specific differences in activity in other vascular cells, including bone marrow-derived macrophages (BMDMs) or endothelial cells (ECs) **(Supplemental Figure 1 C-D)**. Next, to test the effect of the rs62059712 variant on *JMJD3* expression, we used CRISPR-Cas9 to delete the 450 bp region encompassing the SNP in HuSMCs. Deletion of this region resulted in decreased *JMJD3* expression, further supporting the role of rs62059712 in regulating *JMJD3* expression **(Figure 1D)**.

To define the mechanism whereby the rs62059712 minor C allele resulted in increased transcriptional activity, we analyzed the region of the *JMJD3* gene containing the rs62059712 C allele sequence for predicted TF binding sites using the JASPAR web-based tool (37). We found the C-containing sequence conformed to a predicted SP1 binding site **(Figure 1E)**. Additionally, conservation analysis revealed that the region containing the SP1 binding site was conserved

across rodent species, although the major T allele-containing sequence was conserved **(Table 2)**. We performed affinity purification of TFs in HuSMC nuclear lysates using biotin-tagged DNA oligonucleotides that corresponded to rs62059712 minor C, major T, or scrambled negative control sequences. The minor C allele bound the TF, SP1, with greater affinity than the major T allele **(Figure 1F)**. Because SP1 can interact with the TF SMAD2 to drive TGFβ-dependent *ACTA2* expression and because the SMAD family of TFs are known regulators of TGFβ-dependent SMC differentiation, we examined if SMAD2 immunoprecipitated with the C-minor allele probe (10). We found increased SMAD2 binding to the C-containing sequence compared to the T-containing sequence **(Supplemental Figure 1E)**. Next, we used chromatin immunoprecipitation (ChIP) in mAoSMCs to demonstrate Sp1 binding at the *Jmjd3* promoter *in vivo* **(Figure 1G)**. Furthermore, given that TGFβ is a known driver of SMC differentiation, we assessed the effect of TGFβ treatment on Sp1 binding to the *Jmjd3* promoter (11, 38). As demonstrated in **Figure 1H**, Sp1 binding to the murine *Jmjd3* promoter was increased in ChIP experiments following TGFβ stimulation of mAoSMCs. To determine if Sp1 mediated the increased transcription activity of the minor C allele, we transfected DHS1-T major and -C minor allele luciferase constructs in mAoSMCs treated with siRNA against *Sp1* or a non-targeting control (NTC) siRNA. Interestingly, Sp1 knockdown in mAoSMCs abolished the increased transcriptional activity of the C minor allele, decreasing it to that of the T major allele **(Figure 1I)**. Additionally, TGFβ stimulation of mAoSMCs resulted in a 2-fold increase in luciferase activity of the DHS1-C fragment **(Figure 1J)**. Since the DHS1 region was required for *JMJD3* transcription (see Figure 1D) and SP1 binding to this region mediated its allele-specific activity in SMCs, we hypothesized that SP1 was required for *JMJD3* expression. We performed siRNA knockdown of Sp1 in mAoSMCs and measured *Jmjd3* expression. Sp1 knockdown significantly decreased *Jmjd3* expression in mAoSMCs **(Figure 1K)**. Additionally, because SMAD2 also bound the *JMJD3* minor C allele, perhaps via its interaction with SP1, we tested whether SMAD2 regulated *JMJD3*

expression. siRNA knockdown of Smad2 decreased *Jmjd3* expression in mAoSMCs **(Supplemental Figure 1F)**. Taken together, these results demonstrate that the BP-associated human variant rs62059712 minor C allele increases *JMJD3* transcription in SMCs via increased SP1 binding.

JMJD3 loss in vascular smooth muscle cells results in hypertension

Given our identification of a BP-associated gene regulatory region within the human *JMJD3* promoter that displayed allele-specific activity in vascular SMCs, we hypothesized that JMJD3 was required for SMC-mediated vasomotor tone and BP. To determine the role of JMJD3 in SMCs in BP, we created a SMC-specific Jmjd3 deletion murine model by crossing our $Jmjd3^{flox/flox}$ mice (along with $Jmjd3^{WT/WT}$ and $Jmjd3^{flox/WT}$ mice) with tamoxifen-inducible $Myh11^{CreERT}$ mice (to generate $Jmjd3^{flox/flox}Myh11^{CreERT}$ mice) **(Figure 2A)**. To eliminate the effect of tamoxifen on BP and test the roles of heterozygous and homozygous *Jmjd3* deletion, we treated all $Jmjd3^{WT/WT}Myh11^{CreERT}$, $Jmjd3^{flox/WT}Myh11^{CreERT}$, and $Jmjd3^{flox/flox}Myh11^{CreERT}$ littermates with tamoxifen for 5 days, followed by a 3-day "washout" period, to generate WT, $Jmjd3^{flox/WT}Myh11^{Cre+}$, and $Jmjd3^{flox/flox}Myh11^{Cre+}$ mice, respectively. We then implanted osmotic minipumps (ALZET, Model 2004) filled with saline or Angiotensin II and measured BP for 14 days in response to saline or Angiotensin II infusion (1 ug/kg/min). SMC-specific deletion of *Jmjd3* (in $Jmjd3^{flox/flox}Myh11^{Cre+}$ mice) resulted in significantly higher systolic blood pressure (SBP), diastolic blood pressure (DBP), and mean arterial pressure (MAP) in response to Angiotensin II compared to heterozygote and wild-type controls **(Figures 2B-D)**. $Jmjd3^{flox/flox}Myh11^{Cre+}$ mice had significantly increased 14-day averaged SBP, DBP, and MAP compared to littermate controls **(Supplemental Figures 2A-C)**. Because BP is regulated by non-SMC vascular cells (e.g., endothelial cells), we generated endothelial- ($Jmjd3^{flox/flox}Cdh5^{CreERT}$) and myeloid- ($Jmjd3^{flox/flox}Lyz2^{Cre}$) specific murine models of Jmjd3 deletion and measured their BPs. Importantly, Jmjd3 deletion in ECs or myeloid cells did not significantly affect BP **(Supplemental Figures 2D-I)**.

Since arterial SMCs are the main cell type regulating vascular tone/BP, we hypothesized that JMDJ3 deletion resulted in increased vascular SMC contractility, thereby leading to increased arterial tone/BP. SMC contraction occurs after activation of calcium/calmodulin-dependent phosphorylation of myosin light chain kinase, resulting in myosin light chain 2 (pMLC2) phosphorylation (3). Thus, as an index of SMC contractility, we measured pMLC2 via western blotting and found it was increased in human aortic SMCs (HuAoSMCs) treated with a JMJD3 specific inhibitor (GSKJ4, 50 nM) plus Angiotensin II (100 nM) compared to Angiotensin II only (control) **(Figure 2E)**. To elucidate the mechanism of JMJD3-dependent SMC contractility and BP, we performed RNA sequencing (RNA-seq) on cultured aortic SMCs isolated from *Jmjd3*$^{flox/flox}$*Tagln*^{Cre} mice. *Jmjd3* mRNA levels in *Jmjd3*$^{flox/flox}$*Tagln*$^{Cre+}$ SMCs were nearly 100% depleted **(Supplemental Figure 3A)**. Interestingly, among the many genes differentially regulated, we identified several canonical SMC-specific genes (*TAGLN, CNN1, MYH11, SRF, MKL2*) that were strongly downregulated in *Jmjd3*$^{flox/flox}$*Tagln*$^{Cre+}$ SMCs **(Figure 2F)**. SMC-specific marker proteins in aortic tissue from *Jmjd3*$^{flox/flox}$*Tagln*$^{Cre+}$ mice was also decreased **(Supplemental Figure 3B)**. In our RNA-seq data, *Klf4*, a TF that represses SMC differentiation, was upregulated in *Jmjd3*$^{flox/flox}$*Tagln*$^{Cre+}$ SMCs compared to *Jmjd3*$^{flox/flox}$*Tagln*$^{Cre-}$ SMCs (see Fig. 2F). Given the importance of endothelin signaling in SMCs in BP regulation, we examined endothelin receptor expression in our RNA-seq data and identified a 6-fold downregulation in endothelin receptor B (*Ednrb*) expression and 6-fold upregulation in endothelin receptor A (*Ednra*) in *Jmjd3*$^{flox/flox}$*Tagln*$^{Cre+}$ SMCs **(Figure 2G)**. Other genes associated with HTN including *AGTR1A* and *AGT* were increased in *Jmjd3*$^{flox/flox}$*Tagln*$^{Cre+}$ SMCs (see Fig. 2F). Gene ontology (GO) analysis of our RNA-seq results identified common pathways of migration, vascular development, angiogenesis, and signal transduction that were downregulated in *Jmjd3*$^{flox/flox}$*Tagln*$^{Cre+}$ SMCs compared to control **(Figure 2H)**. Complementary GO analysis of upregulated genes in *Jmjd3*$^{flox/flox}$*Tagln*$^{Cre+}$ SMCs revealed pathways common to DNA and RNA processes

(Supplemental Figure 3C). Taken together, JMJD3 in SMCs regulates contractility and BP and controls expression of genes associated with SMC phenotype and HTN.

JMJD3 is required for EDNRB expression in SMCs and suppresses the hypertensive gene program

To further analyze the downstream transcription targets of JMJD3 that drive BP regulation in vascular SMCs, we performed a superarray of well-established genes involved in HTN in aortic SMCs isolated from *Jmjd3*$^{flox/flox}$*Tagln*^{Cre} mice. In alignment with our RNA-seq data, there was a 150-fold reduction in expression *Ednrb* in *Jmjd3*$^{flox/flox}$*Tagln*$^{Cre+}$ SMCs and upregulation of genes known to increase BP (e.g., *Ednra, Agt, Ace2*) **(Supplemental Figure 4A)**. Superarray results were confirmed using qPCR, which demonstrated decreased *Ednrb* expression (and increased expression of HTN genes) in *Jmjd3*$^{flox/flox}$*Tagln*$^{Cre+}$ SMCs **(Figure 3A, Supplemental Figure 4B-H)**. Further, siRNA knockdown of Jmjd3 in mAoSMCs led to increased HTN gene expression, including *Edn1* **(Supplemental Figure 4I, J).** To further examine the regulation of *EDNRB* by JMJD3, we performed siRNA knockdown of Jmjd3 in mAoSMCs and found reduced *Ednrb* expression compared to a non-targeting control (NTC) siRNA **(Figure 3B)**. Notably, because SP1 was required for *JMJD3* transcription, we tested if SP1 played a similar role in regulating endothelin receptor expression. Interestingly, siRNA knockdown of Sp1 in mAoSMCs resulted in increased *Ednra* expression **(Supplemental Figure 5)**. To examine regulation of *EDNRB* by JMJD3 *in vivo*, we harvested aortas from tamoxifen-injected *Jmjd3*$^{flox/flox}$*Myh11*^{CreERT} (*Jmjd3*$^{flox/flox}$*Myh11*$^{Cre+}$) and *Jmjd3*$^{WT/WT}$*Myh11*^{CreERT} (WT) mice after 14-day treatment with Angiotensin II (as described above in tail cuff BP experiments) and found reduced *Ednrb* expression in aortas from mice with SMC-specific *Jmjd3* deletion **(Figure 3C)**. Notably, increased Ednrb protein in aortic tissue in response to Angiotensin II was abolished by SMC-specific *Jmjd3* deletion **(Figure 3D)**. *Ednrb* in aortas was also increased at the mRNA level by Angiotensin II treatment **(Figure 3E)**. We tested the effects of EDNRB loss on downstream endothelin and HTN signaling using siRNA-mediated knockdown of Ednrb in mAoSMCs, which led to increased HTN

gene expression **(Figure 3F-I)**. To determine whether the effects on *Ednrb* expression after Jmjd3 deletion were due to changes in H3K27me3, the epigenetic mark associated with Jmjd3, we performed ChIP in mAoSMCs from *Jmjd3*$^{flox/flox}$*Tagln*^{Cre} mice and observed increased H3K27me3 at the *Ednrb* promoter in Jmjd3-deficient SMCs **(Figure 3J).** Additionally, H3K27me3 enrichment was increased at the *Ednrb* promoter in mAoSMCs treated with *Jmjd3* siRNA compared to NTC siRNA **(Figure 3K)**. Next, to determine if the relationship between *JMJD3* and *EDNRB* expression was conserved in human SMCs, we isolated femoral arteries from four HTN patients. scRNA-seq and Pearson correlation analysis identified significant correlation between *JMJD3* and *EDNRB* in SMCs **(Figure 3L)**. Since there are two endothelin receptors (A and B) and prior reports have identified dual roles for these receptors, we examined if *EDNRA* expression levels were altered relative to *JMJD3* (3). In both our superarray (see Supplemental Fig. 4A) and targeted qPCR in *Jmjd3*$^{flox/flox}$*Tagln*^{Cre} SMCs, we found increased *Ednra* expression in mAoSMCs after *Jmjd3* depletion **(Figure 3M)**. We also observed increased Ednra by immunofluorescent staining of *Jmjd3*$^{flox/flox}$*Myh11*$^{Cre+}$ aortas compared to aortas from WT mice **(Figure 3N)**. Additionally, Ednra protein was increased in *Jmjd3*$^{flox/flox}$*Tagln*$^{Cre+}$ SMCs **(Figure 3O)**. Next, we performed siRNA knockdown of *Ednrb* in mAoSMCs and measured *Ednra* expression by qPCR. Interestingly, Ednrb knockdown led to a 4-fold increase in *Ednra* expression in mAoSMCs, suggesting an intricate transcriptional balance between *EDNRA* and *EDNRB* that is controlled by JMJD3 **(Figure 3P)**. In sum, these results show JMJD3, likely via EDNRB, regulates SMC contractility and BP.

JMJD3 regulates vessel tone via endothelin-ERK signaling in vascular smooth muscle cells

Since BP control is complex and regulated by multiple organ systems, we tested the effects of JMJD3 deletion on vessel tone independent of organ tissues. We isolated aortic and mesenteric artery segments from *Jmjd3*$^{flox/flox}$*Myh11*^{CreERT} mice injected with tamoxifen (*Jmjd3*$^{flox/flox}$*Myh11*$^{Cre+}$) or corn oil (*Jmjd3*$^{flox/flox}$*Myh11*$^{Cre-}$) and measured their contractility using a vessel ring assay in response to various contractile agonists, including endothelin-1 (ET-1),

angiotensin II (Ang II), and phenylephrine (PE), *ex vivo*. We observed that aortas isolated from *Jmjd3*$^{flox/flox}$*Myh11*$^{Cre+}$ mice exhibited increased vessel tone compared to *Jmjd3*$^{flox/flox}$*Myh11*$^{Cre-}$ littermate controls in response to ET-1 (10^{-7} M), and this was negated by treatment with the dual endothelin receptor antagonist, bosentan (10^{-8} M) **(Figure 4A)**. This was also observed in mesenteric arteries, and although *Jmjd3*$^{flox/flox}$*Myh11*$^{Cre+}$ mesenteric arteries displayed higher baseline contractility than *Jmjd3*$^{flox/flox}$*Myh11*$^{Cre-}$ littermate controls, there was no difference in response to Ang II or PE **(Figure 4B)**. This indicated that the effects of JMJD3 deletion on vessel tone were specific to endothelin signaling rather than other vasoactive agonists. In agreement with this, *Jmjd3*$^{flox/flox}$*Myh11*$^{Cre+}$ aortas exhibited increased responsiveness to ET-1 stimulation compared to aortas isolated from *Jmjd3*$^{flox/flox}$*Myh11*$^{Cre-}$ controls, and this enhancement in contractility was reduced to *Cre-* baseline levels following bosentan treatment **(Figure 4C)**.

Next, to directly test the effect of JMJD3 deletion on SMC contractility, we utilized a collagen gel contraction assay in which aortic SMCs were isolated from *Jmjd3*$^{flox/flox}$*Tagln*^{Cre} mice and embedded in a collagen gel, treated with ET-1 (1 uM) and/or bosentan (10 uM), and gel area was measured. Gels containing *Jmjd3* deficient mAoSMCs had smaller areas compared to control SMCs in response to ET-1, and treatment of gels containing SMCs deficient in *Jmjd3* with bosentan resulted in gel areas comparable to untreated gels **(Figure 4D)**. Taken together, these results suggest that JMJD3 deletion results in increased SMC contraction via endothelin signaling, leading to increased arterial tone and BP.

Endothelin receptor stimulation results in ERK pathway activation, leading to SMC contraction (3, 39, 40). Supportive of this, treatment of HuAoSMCs with ET-1 (1 uM) for 5 minutes led to increased pERK, which was increased further by pre-treatment of SMCs with the JMJD3 inhibitor GSKJ4 (50 nM) **(Figure 4E)**. Next, we treated *Jmjd3*$^{flox/flox}$*Tagln*^{Cre} SMCs with ET-1 (1 uM) with or without the endothelin receptor antagonist bosentan (10 uM) and then measured pERK by western blotting. As shown in **Figure 4F**, baseline ERK activity was modestly increased in Jmjd3-deficient SMCs compared to *Jmjd3*$^{flox/flox}$*Tagln*$^{Cre-}$ SMCs, and treatment with ET-1

resulted in a substantial increase in pERK in Jmjd3-deficient SMCs compared to controls. Pre-treatment of mAoSMCs with bosentan resulted in a small reduction in pERK activity in Jmjd3-deficient mAoSMCs. We also observed increased pERK in *Jmjd3*$^{flox/flox}$*Tagln*$^{Cre+}$ SMCs compared to control SMCs via immunofluorescence **(Figure 4G)**. Additionally, in immunofluorescence experiments, overexpression of flag-JMJD3 in mAoSMCs led to decreased pERK activity in mAoSMCs treated with Ang II (100 nM) **(Figure 4H)**. Taken together, these results demonstrate that JMJD3 regulates endothelin-pERK signaling in SMCs.

To delineate the translational impact of enhanced endothelin signaling (specifically endothelin receptor A) on BP after JMJD3 deletion in SMCs, we tested BP response in *Jmjd3*$^{flox/flox}$*Myh11*^{Cre} mice treated with the FDA-approved endothelin receptor A-specific antagonist, BQ-123. As observed above, *Jmjd3*$^{flox/flox}$*Myh11*$^{Cre+}$ mice exhibited increased SBP, DBP, and MAP compared to *Cre-* littermate controls. However, treatment of *Jmjd3*$^{flox/flox}$*Myh11*$^{Cre+}$ mice with BQ-123 (200 nmol/kg/day) normalized BP to *Cre-* levels **(Figure 5A-C)**. As above, knockdown of Jmjd3 in mAoSMCs led to upregulation of key HTN genes (see Supp. Fig. 4J), which was inhibited by treatment of mAoSMCs *in vitro* with BQ-123 (5 uM) **(Figure 5D)**.

JMJD3 is required for vascular smooth muscle cell differentiation

During long-standing HTN SMCs transition from a contractile to synthetic phenotype (41, 42). Given the role of JMJD3 in SMCs on BP *in vivo*, we investigated if SMC phenotype is altered by JMJD3. We examined mAoSMCs for *Jmjd3* expression after stimulation with TGFβ (20 ng/ml), since TGFβ is a well-established driver of SMC differentiation (11). TGFβ increased *Jmjd3* expression in mAoSMCs by approximately 2-fold **(Figure 6A)**. Next, we performed ChIP for Jmjd3 on mAoSMCs at canonical SMC-specific gene promoters (*Acta2, Tagln, Cnn1, Myh11*). Jmjd3 demonstrated significant enrichment at smooth muscle gene promoters in mAoSMCs **(Figure 6B)**. Next, we used siRNA-mediated knockdown of Jmjd3 in mAoSMCs treated with TGFβ (20 ng/ml) to investigate the effect of Jmjd3 on SMC-specific gene expression (*Acta2, Tagln, Cnn1,*

Myh11). Jmjd3 knockdown reduced TGFβ-dependent expression of SMC genes (*Acta2, Tagln, Myh11*) at the mRNA and protein levels compared to control NTC siRNA **(Figures 6C, D)**. To examine this genetically, we analyzed smooth muscle gene expression in $Jmjd3^{flox/flox}Tagln^{Cre}$ SMCs. SMC gene expression was significantly reduced in $Jmjd3^{flox/flox}Tagln^{Cre+}$ SMCs compared to *Cre-* SMCs **(Figure 6E)**. Further, pharmacologic treatment of mAoSMCs with the Jmjd3 selective inhibitor GSKJ4 (50 nM) inhibited smooth muscle gene expression (*Acta2, Tagln, Cnn1, Myh11*) **(Figure 6F)**. To examine the direct effects of Jmjd3 on SMC gene promoters, ChIP was performed for H3K27me3 in mAoSMCs treated with siRNA to *Jmjd3* or NTC siRNA. Jmjd3 knockdown resulted in increased H3K27me3 enrichment at SMC-specific gene promoters (*Acta2, Tagln, Cnn1, Myh11*), indicating that JMJD3 positively regulates SMC gene expression directly by removing H3K27me3 from gene promoters **(Figure 6G-J)**. These results reveal that *JMJD3* expression is increased by TGFβ and required for SMC gene expression via an H3K27me3-mediated mechanism.

Given our findings that JMJD3 loss in SMCs increased endothelin signaling and ERK activation, as well as evidence from others demonstrating that increased ERK activity represses SMC gene expression, we explored whether JMJD3 controlled SMC gene expression via ERK signaling (43). First, as a translational corollary, treatment of HuSMCs with the ERK inhibitor SCH772984 (5 uM) robustly increased SMC gene expression (*ACTA2, CNN1, MYH11*) **(Figure 6K)**. Next, to examine ERK inhibition after JMJD3 loss, we treated mAoSMCs with combinations of GSKJ4 (50 nM), ET-1 (1 uM), and/or SCH772984 (5 uM). ET-1 treatment significantly reduced SMC gene expression, which was further decreased by inhibiting Jmjd3 with GSKJ4 (50 nM). Treatment of mAoSMCs with SCH772984 (5 uM) prevented downregulation of SMC gene expression by ET-1 (1 uM) and GSKJ4 (50 nM) alone and in combination with each other **(Figure 6L-N)**. These data reveal that JMJD3 loss results in decreased smooth muscle gene expression

via increased H3K27me3 at SMC gene promoters and by increased endothelin-ERK activation, inhibition of which restores SMC gene expression **(Figure 6O)**.

Hypertensive-induced arterial remodeling is regulated by JMJD3

We show that JMJD3 regulates SMC differentiation and endothelin/ERK signaling, which both control SMC phenotype. Thus, we examined the role of JMJD3 in SMCs on arterial remodeling during long-standing HTN. Since BP is regulated by resistance arteries, we measured renal arteriole wall thickness from *Jmjd3*$^{flox/flox}$*Myh11*$^{Cre+}$ and WT mice treated with Angiotensin II for 14 days and observed increased media to diameter ratio in mice with SMC-specific deletion of Jmjd3 compared to littermate controls, indicating increased remodeling (i.e. increased migration and phenotypic modulation) **(Figure 7A, B)**. We assessed arterial beds from different vascular tissues under basal (saline) and Ang II-treated conditions and observed increased remodeling after Jmjd3 deletion in SMCs was most exaggerated in smaller resistance arteries (renal arterioles) in Ang II-treated mice and overall unaffected in larger, conduit arteries (aorta) **(Fig. 7A, B, Supplemental Figure 6)**. Since Angiotensin II induces SMC phenotypic modulation and arterial remodeling, we explored whether Ang II regulates JMJD3 expression, thereby leading to changes in SMC gene expression during HTN (41, 44). We first measured *Jmjd3* mRNA in aortas isolated from mice treated with saline or Ang II and observed decreased *Jmjd3* expression in aortas from Ang II-treated mice **(Figure 7C)**. This was accompanied by reduced expression of *Acta2, Tagln, Cnn1, and Myh11* in whole aorta tissue **(Figures 7D)**. Given that JMJD3 was required for SMC differentiation (see Figure 6), we examined if JMJD3 regulated SMC gene expression during Angiotensin II-mediated hypertensive arterial remodeling. We measured smooth muscle gene expression (*Acta2, Tagln, Cnn1, Myh11*) in *Jmjd3*$^{flox/flox}$*Myh11*$^{Cre+}$ and WT mice treated with Angiotensin II for 14 days. SMC-specific Jmjd3 deletion resulted in further loss of SMC markers (both mRNA and protein) in aortas from Ang II-treated mice **(Figures 7E, F)**. The TF KLF4 controls the SMC switch from the mature, contractile to the proliferative, synthetic phenotype, thus we examined if *KLF4* expression was altered under hypertensive conditions (12,

15). Indeed, Angiotensin II (100 nM) increased *KLF4* expression in HuAoSMCs *in vitro*, suggesting that KLF4 may drive phenotypic modulation during hypertensive remodeling **(Figure 7G)**. Because loss of JMJD3 promoted the synthetic SMC phenotype, we tested if KLF4 was transcriptionally regulated by JMJD3. First, we *Klf4* expression was upregulated 2.5-fold in *Jmjd3*$^{flox/flox}$*Tagln*$^{Cre+}$ mAoSMCs compared to littermate *Cre*- controls **(Figure 7H)**. Additionally, siRNA knockdown of Jmjd3 in mAoSMCs increased *Klf4* expression nearly 3-fold compared to NTC siRNA **(Figure 7I)**. This was supported by scRNA-seq of aortas from saline versus Ang II-treated *Jmjd3*$^{flox/flox}$*Myh11*^{Cre} mice, in which Ang II decreased *Jmjd3* expression and increased *Klf4* expression, which was further increased by Jmjd3 deletion **(Figure 7J).** Interestingly, GO analysis of DEGs in SMCs from these mice demonstrated that Jmjd3 loss in chronic HTN results in increased expression of genes related to tissue injury, actin cytoskeleton, AKT signaling, and inflammation, some of which are known downstream targets of ET-1 signaling **(Figure 7K)**. SMC migration, which is regulated by ERK signaling and phenotypic modulation, was increased in *Jmjd3*$^{flox/flox}$*Tagln*$^{Cre+}$ SMCs in scratch assays (smaller wound area remaining in *Cre*+ SMCs) **(Figure 7L)**. In summary, Angiotensin II-induced downregulation of *JMJD3* in SMCs results in loss of mature SMC genes and increased *KLF4*, which cooperatively drive phenotypic modulation and remodeling during long-standing HTN **(Figure 7M).**

JMJD3 regulates the contractile gene program in SMCs by cooperatively regulating SRF binding to SMC gene promoters

In order to translate the above *in vivo* murine findings to humans, we performed scRNA-seq in human femoral artery samples (n=4) **(Figure 8A)**. First, we measured *JMJD3* expression in SMCs from human arteries and found *JMJD3* was expressed in SMCs at moderate levels **(Figure 8B)**. Next, we performed Pearson expression correlation analysis among genes associated with contractile and synthetic gene programs in SMCs. As shown in **Figure 8C**, genes associated with mature, contractile SMC phenotype including *ACTA2, TAGLN, CNN1,* and *MYH11* showed very strong correlation with one another, yet weak or no correlation with synthetic,

proliferative-associated genes including *PDGFBR, PDGFB, KLF4,* and *ETS-1*. Similarly, the proliferative genes exhibited strong correlation with each other. The distinct clustering of mature genes and proliferative genes confirmed the utility of this approach. Next, we performed analysis of *JMJD3* expression in SMC subsets separated into high or low expression of contractile genes. We found that *JMJD3* expression (as was the number of JMJD3-expressing cells) was increased in *ACTA2* and *CNN1* "high" SMCs compared to "low"-expressing SMCs **(Figure 8D)**. Because CMEs cooperatively regulate TF binding, we investigated whether JMJD3 affected SRF binding to SMC gene promoters. We performed ChIP for Srf at SMC gene promoters in mAoSMCs treated with *Jmjd3* siRNA or NTC siRNA. We observed decreased binding of Srf to *Acta2*, *Tagln*, and *Cnn1* promoters in Jmjd3 knockdown mAoSMCs compared to control **(Figure 8E)**. Taken together, our data reveal that JMJD3 regulates the contractile gene program in human SMCs and cooperatively affectgs SRF binding at smooth muscle gene promoters.

Discussion

Here, we define the mechanistic pathway linking the BP-associated polymorphism rs62059712 to transcriptional regulation of *JMJD3*, which regulates endothelin-dependent BP and SMC phenotype via epigenetic alterations at gene promoters and changes in ERK signaling. This work uncovers an allele-specific mechanism regulating expression of an epigenetic enzyme (JMJD3) that controls endothelin receptor expression, and consequently, modulates SMC contractility, differentiation, and arterial remodeling in response to long-standing HTN. These findings identify a key pathway linking genetic and epigenetic mechanisms to molecular control of SMC function and phenotype, thereby revealing how GWAS and similar studies can be used to identify new epigenetic regulators of disease. The rs62059712 major T allele is associated with increased use of medications acting on the renin-angiotensin system, diuretics, and calcium channel blockers (Supplemental Table 1). Thus, the rs62059712 genotype-JMJD3 interaction may yield insight into genetic response to current anti-hypertensive therapies. Interestingly, the major T allele, which is associated with increased BP, is conserved across rodent species, indicating that the minor C allele confers a protective advantage despite its lower frequency in the population.

We characterize the effect of rs62059712 on *JMJD3* transcription, demonstrating that the minor C allele increases *JMJD3* promoter activity by creating an SP1 binding site within this region. SP1 loss phenocopied loss of JMJD3 in SMCs, indicating the important role of this TF in mediating downstream effects on gene expression. SP1 induces the SMC phenotypic switch after vascular injury by directly binding to GC repressor elements in SMC-specific genes (e.g., *MYH11*) as well as indirectly by increasing expression of *KLF4*, which inhibits myocardin function and downstream SMC differentiation (10, 12). In contrast, reports have demonstrated positive effects of SP1 on gene transcription, for example, increasing *ACTA2* expression in myofibroblasts (10). Furthermore, interactions involving other epigenetic complexes, such as p300 and acetylated histone 3, cooperatively regulate SP1 function to refine its transcriptional effect on SMCs (45).

Thus, SP1 may control HTN gene expression via additional cooperative mechanisms, perhaps by interacting with SMAD2, which was partially investigated here. Additionally, JMJD3 influences SRF binding to SMC gene promoters, and identification of additional co-regulators of JMJD3 will provide further insight into epigenetic regulation of SMC phenotype in disease.

While SMCs are the main determinant of BP, other cell types play a role. In our study, despite JMJD3's expression in other vascular cell types (e.g., myeloid cells), the allele-specific mechanism was only observed in SMCs, and loss of JMJD3 in non-SMC cell types did not affect BP. We use non-invasive measurements of BP, which we acknowledge can be variable. However, the differences in BP in Jmjd3 deficient versus WT mice were observed at individual days as well as when averaged over the course of the experiment. Further, repeat experiments corroborated our findings demonstrating increased BP in mice with SMC-specific Jmjd3 loss.

BP regulation is controlled by numerous upstream molecular, genetic, and epigenetic signals. GWAS have provided insight into the genetic regulation of BP through identification of candidate variants associated with BP (46, 47). At least three SNPs have been identified that influence endothelin signaling. rs9349379, located in an intron within the *PHACTR1* gene, affects *ET1* expression by altering long-range gene interactions between *PHACTR1* and *ET1* (48). Additionally, rs1630736 in the *ET1* gene, and rs10305838 in the *EDNRA gene*, are associated with BP (49, 50). Here, we find that JMJD3 loss in SMC leads to increased endothelin-ERK signaling, resulting in decreased SMC gene expression. Our results suggest that targeting ERK in long-standing HTN, and perhaps other models of vascular injury, may limit pathologic arterial remodeling. Keaton et al. reported a 0.47 mmHg increase in systolic BP for each copy of the major allele (29). While this per copy allele effect is seemingly small, albeit typical for similar reported SNPs, it is likely that this SNP interacts with other genetic, epigenetic, and molecular signals to create larger changes in BP.

While prior studies have investigated the role of epigenetic alterations in cardiovascular disease, the exact role of H3K27me3 in HTN remains unknown (20-25, 27). Increased H3K27me3

levels have been associated with BP (51). We show that H3K27me3 enrichment at *EDNRB*, *ACTA2*, *TAGLN*, *CNN1*, and *MYH11* gene promoters is regulated by JMJD3, and future studies will determine how H3K27me3 at these promoters changes in the setting of HTN. Our identification of *EDNRB* as a direct transcriptional target of JMJD3 is consistent with reports that have identified that *EDNRB* expression is positively regulated by SMC-specific TFs (e.g., MKL2) (52). While SMCs are the predominant cell type regulating vessel tone and BP, endothelin signaling involves interplay between SMCs and endothelial cells (ECs). Therefore, JMJD3 in SMCs and ECs may synergistically regulate arterial remodeling during HTN. Finally, deletion of JMJD3 led to increased HTN-associated genes, including endothelin-1 (ET-1/*EDN1*). Thus, loss of JMJD3 may create a feed forward mechanism whereby increased endothelin-1 and other HTN-associated genes worsens HTN.

We demonstrate that the rs62059712 major T allele decreases *JMJD3* expression, mechanistically resulting in a "double hit," first leading to increased BP via increased *EDNRA* expression, and next, resulting in increased pathologic remodeling due to increased ERK signaling and H3K27me3 at smooth muscle gene promoters. In our analysis of different vascular beds, we observed significant differences in media thickness in Angiotensin II-treated mice, which was not as prominent under basal conditions. This suggests that regulation of arterial remodeling by JMJD3 requires a "second hit," such as prolonged HTN. Although we observed differences in downstream gene expression and BP under basal conditions (i.e. saline treatment), this did not translate to changes in remodeling phenotype under basal conditions.

Blood pressure is a complex phenotype controlled by multiple factors. Our study reveals that the rs62059712 major T allele decreases *JMJD3* transcription in SMCs by disrupting SP1 binding to the *JMJD3* promoter, leading to decreased *JMJD3* expression. We identify the *EDNRB* gene as a direct transcriptional target of JMJD3, which is decreased by the major T allele, thereby resulting in compensatory increase in *EDNRA* expression. Thus, loss of *JMJD3* increases endothelin signaling and downstream vessel contractility. Specific inhibition of Endothelin A

receptor normalized the increased BP resulting after JMJD3 loss in SMCs. Decreased *JMJD3* further negatively modifies disease phenotype by leading to increased ERK activation, which increases SMC migration and phenotypic modulation during pathologic arterial remodeling. In conclusion, our findings define a unique transcriptional and molecular axis involving the histone demethylase, JMJD3, in SMCs that regulates blood pressure and arterial response to injury.

Methods

Sex as a biological variable. For BP experiments using *Jmjd3*$^{flox/flox}$*Myh11*^{CreERT} mice, only male mice were used because the *Myh11*^{CreERT} transgene is located on the Y chromosome.

Animals. Animal studies were approved by the Animal Care Committee of the University of Michigan and complied with the National Institutes of Health (NIH) guide for the care and use of laboratory animals. Mice were housed in stock-holding rooms under pathogen-free conditions. *Jmjd3*$^{flox/flox}$*Myh11*^{CreERT}, *Jmjd3*$^{flox/flox}$*Tagln*^{Cre}, *Jmjd3*$^{flox/flox}$*Cdh5*^{CreERT}, and *Jmjd3*$^{flox/flox}$*Lyz2*^{Cre} mice were bred on a C57BL6/J background, and experiments were performed on 8-12 week old mice. For inducible deletion of *Jmjd3* in SMCs and ECs, mice were injected intraperitoneally with tamoxifen (75 mg/kg) for 5 consecutive days, then allowed a 3-day washout period before experiments. Mice had free access to water and food throughout the study.

Angiotensin II infusion and non-invasive blood pressure measurements. Osmotic mini-pumps (ALZET, Model 2004) containing saline or Angiotensin II were inserted subcutaneously in mice as previously described (30). Angiotensin II was infused at a rate of 1 ug/kg/min. Mice were allowed to recover for 1 day before measuring BP. Daily BP measurements were obtained using noninvasive tail-cuff system (Kent Scientific). Animals were allowed to equilibrate in the system and at least two cycles of preliminary BP measurements were performed to ensure accurate recording. BP was measured daily through day 14 at which time mice were sacrificed and tissues harvested for downstream analysis. In Endothelin receptor A inhibitor experiments, mice were treated with BQ-123 (200 nmol/kg/day) each day beginning day 8 of BP measurements.

Aortic and mesenteric artery ring contractility assays. Aortas and mesenteric arteries were isolated after 5 days of intraperitoneal tamoxifen (75 mg/kg) or corn oil injection of *Jmjd3*$^{flox/flox}$*Myh11*^{CreERT}mice, following a 3-day washout period. For each mouse, vessels were cut into two rings and run in parallel. Aortic and mesenteric rings were mounted vertically on two wire hooks and immersed in 2 ml KH buffer (in mM: 118 NaCl, 4.8 KCl, 1.2 MgSO4, 1.2 KH2PO4, 25 NaHCO3, 11 glucose, and 2.5 CaCl2; pH 7.4, maintained with 95% O2-5% CO2 at 37C. Vessel

rings were equilibrated for 90 min with a resting tension of 1 g. After baseline tension was determined, vessels were precontracted with 60 mM KCl. Increasing concentrations of endothelin-1 (10^{-10}-10^{-7} M), angiotensin II (10^{-9}-10^{-5} M), and phenylephrine (10^{-9}-10^{-4} M) were used. Concentration of bosentan used was 10^{-8} M. Values were normalized to percent contraction of KCl.

Cell culture. Human aortic and bronchial smooth muscle cells were purchased from Lonza and maintained in Clonetics Smooth Muscle Growth Medium-2 (SMGM-2) supplemented with growth factors, 5% FBS, and antibiotics. Human SMCs were maintained and used for experiments between passages 2 and 14. Primary mouse aortic SMCs (mAoSMCs) were isolated from thoracic aortas of 12-16 week old mice and maintained through passage 14 in DMEM F12 with 10% FBS and 0.5% penicillin and streptomycin.

Plasmids. pGL3-*JMJD3* DHS 1 and 2 major and minor allele reporter constructs were generated by amplifying 600 bp gene regions from a human SMC genomic DNA template. DNA fragments were then cloned into pGL3 luciferase basic vector (Addgene), and the correct sequence was verified by Sanger sequencing. Mutations were introduced using QuickChange site-directed mutagenesis protocol. All mutations were verified by Sanger sequencing. pCS2-Jmjd3-F was a gift from Kai Ge (Addgene plasmid #17440; http://n2t.net/addgene:17440 ; RRID:Addgene_17440).

Luciferase assays. mAoSMCs were seeded in 24-well plates at 2.4 x 10^4 cells/well. Cells were transfected the day after plating with 50 ng of plasmid per well. Luciferase activity was measured 48 h after transfection using the Steady-Glo Luciferase Kit (Promega) according to manufacturer's instructions. Raw luciferase values were normalized to the activity of the pGL3 empty vector.

Gel contractility assays. mAoSMCs were trypsinized when 80% confluent and resuspended at 6×10^5 cells/mL in DMEM F12 with 10% FBS and antibiotics. Cells were diluted in type 1 collagen with DMEM F12 with 10% FBS and 0.5% antibiotics to 1 mg/mL collagen and 3×10^5 cells/mL final concentration. 500 ul of the mixture was added to each well of a 24-well plate. Gels were allowed

to polymerize at 37C for 1 hour. Once gels were polymerized, gels were freed from well edges and 500 ul of media (with or without pharmacologic agent) was added to each well. Collagen gels were incubated for 24 hours, and the area of each gel was measured over time.

Scratch assays. Cells were seeded in a 6-well culture dish and grown to 90% confluence. Cells were treated with 5 ug/ml mitomycin C for 2 hours. A vertical scratch was made in each well with a p200 pipette tip, the media was removed, washed once with PBS, and fresh media was added. Scratch area was measured from 0 hours to 18 hours.

siRNA knockdowns. mAoSMCs were transfected with 40 nM siRNA (Dharmacon) targeted to *Jmjd3*, *Sp1*, *Ednrb*, or a non-targeting control (NTC) siRNA for 72 hours. RNAiMax (Invitrogen) was used as the transfection reagent. Depending on experiment, cells were either left in 10% FBS media, serum starved, or serum starved then treated with agonist or pharmacologic agent.

RNA extraction and qRT-PCR. Cultured SMCs were collected directly in Trizol and RNA was extracted and converted to cDNA using superscript cDNA synthesis kit (Invitrogen). 20-50 ng cDNA was used in downstream quantitative real-time Taqman PCR and normalized using 18S. Tissues were snap frozen, pulverized using mortar and pestle, and collected in trizol. Homogenized tissue was digested into single cell suspension using 20G needle and syringe. Samples underwent RNA extraction and downstream qRT-PCR as above.

Western blotting. Cultured SMCs were lysed in RIPA buffer plus protease and phosphatase inhibitors and 1 mM DTT. Tissues were snap frozen, pulverized, and collected in RIPA buffer with protease and phosphatase inhibitors and 1 mM DTT as above. Lysates were normalized by total protein concentration, sample buffer was added, and then samples were boiled for 5 minutes. 10 to 50 ug of protein was loaded on an SDS-PAGE gel and run. Proteins were transferred to nitrocellulose or PVDF membranes and blocked in either 3% BSA or 5% non-fat dry milk. Blocked membranes were incubated with primary antibodies overnight at 4C. Membranes were washed and incubated with species-specific HRP-linked secondary antibodies, washed, and developed. For densitometry results, Western blots were analyzed using NIH ImageJ software.

Affinity purification of transcription factors. Human aortic SMC nuclear lysates were prepared using the NUPER nuclear extraction kit (ThermoScientific) per manufacturer protocol. Nuclear extracts were diluted with two volumes of 1.3xPD buffer (1x: 10mM Hepes pH 7.4, 8% glycerol, 1mM MgCl2, 0.05% Tritonx100, DTT 1.3 mM, protease and phosphatase inhibitors). 5' biotinylated sense and unmodified anti-sense 25 bp oligos (Sigma) were annealed, added to diluted pre-cleared nuclear lysates, and incubated with rotation for 10 min at room temperature. Streptavidin Dynabeads (Invitrogen) were added to the mixture, incubated for 30 min with rotation, and then beads were washed. Complexes were eluted in 2X sample buffer for analysis via SDS-PAGE and Western blotting.

Chromatin Immunoprecipitation (ChIP) experiments. mAoSMCs were fixed for 10 minutes in 0.7% formaldehyde. The crosslinking reaction was quenched by incubating cells with 0.125 M glycine for 5 minutes. ChIP assays were performed using the Abcam ChIP kit (Abcam Cat# ab500) according to manufacturer's instructions. Sheared chromatin was incubated overnight at 4C with 2 ug of JMJD3 antibody (Abcam), H3K27me3 antibody (Active Motif), or normal rabbit IgG antibody (Diagenode). Eluted DNA was used in downstream qPCR assays.

Histology and Immunofluorescence. Tissues were harvested from mice and fixed in 10% formalin for 24 hours then stored in 70% ethanol. Specimens were embedded in paraffin and sectioned onto microscope slides. After deparaffinization, sections underwent hematoxylin and eosin staining or were processed for immunofluorescence. For immunofluorescent staining, slides underwent antigen retrieval in citric acid buffer (pH 6.0). Samples were then permeabilized, blocked, and incubated with primary antibody in blocking solution overnight at 4C in a humidity chamber. Specific antibodies with dilutions and source are listed separately in "Antibodies." The following day, slides were washed in PBS, then incubated with fluorophore-conjugated secondary antibody (1:500) in PBS for 2 hours at room temperature. Slides were washed with PBS, mounted, allowed to dry overnight, and then imaged.

671 ***RNA-seq experiments.*** Cultured SMCs from *Jmjd3*$^{flox/flox}$*Tagln*^{Cre} mice were plated in 6-well
672 plates at approximately 60% confluence. Cells were harvested the day after initial plating. 3
673 biological replicates for each genotype were used. RNA isolation was performed using RNeasy
674 Kit (Qiagen) with DNAse digestion. Library construction and analysis of reads was performed as
675 described previously (53). Briefly, reads were trimmed using Trimmomatic and mapped using
676 HiSAT2 (54, 55). Read counts were performed using the feature-counts option from the subRead
677 package followed by the elimination of low reads, normalization and differential gene expression
678 using edgeR (56, 57). Differential expression was performed on mapped reads using the taqwise
679 dispersion algorithm in edgeR.
680 ***Phenome-wide Association Study***. OpenGWAS (https://gwas.mrcieu.ac.uk/), a database of
681 350 billion genetic associations from 50,044 GWAS summary datasets, and the GWAS Catalog
682 (https://www.ebi.ac.uk/gwas/), a repository of GWAS summary statistics maintained by NHGRI
683 and EBI, were queried for the lead candidate variant, rs62059712. Summary statistics were
684 download and compiled. Phenotypes associated with rs62059712 were noted.
685 ***scRNA-seq experiments.*** Generation of single-cell suspensions for scRNA-Seq was performed
686 as described by our group previously (31). Briefly, following informed consent from patients and
687 in accordance with University of Michigan IRB Study # HUM00098915, femoral artery specimens
688 were harvested during femoral endarterectomy, femoral-femoral bypass, or aorto-bi-femoral
689 bypass operations. Samples were digested overnight at 4C. Cells were strained and then
690 combined in a 1:1 ratio for scRNA-Seq by the University of Michigan Advanced Genomics Core
691 on the 10x Genomics Chromium System. Libraries were sequenced on the Illumina NovaSeq
692 6000 sequencer. NovaSeq was used as the sequencing platform to generate 151 bp paired-end
693 reads. We conducted adapter trimming and quality control procedures as described previously
694 (58). The reads were then mapped using STAR (59) to build human GRCh37, and gene
695 expression levels were quantified and normalized by HTSeq (60) and DESeq2 (61), respectively.

Negative binomial models in DESeq2 were used to conduct differential expression analysis. Data processing, including quality control, read alignment, and gene quantification, was conducted using the 10X Genomics Cell Ranger software. Seurat was then used for normalization, data integration, and clustering analysis (62). All clustered cells were mapped to corresponding cell types by matching cell cluster gene signatures with putative cell type-specific markers.

Statistical Fine Mapping. GWAS summary statistics from Keaton et al. were subsetted to include a 500kb region on chromosome 17 centered about the GWAS lead variant rs62059712 (chr17:7490170-7990170). Statistical fine mapping using Bayes factor analysis was performed for a 99.9% credible set in R using the function calc_credset from the package levinmisc (https://github.com/mglev1n/levinmisc/blob/main/R/calc_credset.R).

Statistics. GraphPad Prism software (RRID:SCR_002798) version 9.2.0 was used to analyze the data. All data were analyzed for normal distribution and then statistical significance between multiple groups was obtained using Student t-tests, ANOVA, or Pearson's correlation where appropriate. All p-values less than or equal to 0.05 were considered significant.

Study approval. All experiments using human samples were approved by the IRB at the University of Michigan (IRB #: HUM00098915) and were conducted in accordance with the principles in the Declaration of Helsinki.

Data Availability. Sequencing data is available using data accession numbers GSE292027 and GSE292037. Data are available from the corresponding author upon request.

Acknowledgements

We thank Robin G. Kunkel for her artistic work.

Sources of Funding

National Institute of Heath grants R01-HL137919, R01-AR079863-01, R01-HL156274-01A1, R01-DK 127531-01A1 (KAG)

Doris Duke Foundation CSDA 2017079 (KAG)

National Institute of Heath grant R01-DK124290-01 (KAG, BBM)

National Institute of Heath grant F32-DK131799-01 (KDM)

American College of Surgeons Resident Research Award (KDM)

Vascular and Endovascular Surgical Society Resident Research Award (KDM)

The Coller Surgical Society Resident Research Award (KDM)

Author contributions

Conceptualization: KDM, KAG

Experimental Design: KDM, LC, AO, FMD, LCT, JG, KAG, SD

Performed experiments: KDM, LQ, KH, TB, SJW, JS, JYM, ECB, ADJ, ZA, RW, KB

Data analysis: KDM, LQ, KH, ADJ, RW, LCT, SD

Figures: KDM, LQ, KH, SD

Writing: KDM, KAG, SD

Funding acquisition: KDM, KAG

Disclosures: None

References

1. Whelton PK, Carey RM, Aronow WS, Casey DE, Collins KJ, Dennison Himmelfarb C, et al. 2017 ACC/AHA/AAPA/ABC/ACPM/AGS/APhA/ASH/ASPC/NMA/PCNA Guideline for the Prevention, Detection, Evaluation, and Management of High Blood Pressure in Adults: Executive Summary: A Report of the American College of Cardiology/American Heart Association Task Force on Clinical Practice Guidelines. Circulation. 2018;138(17):e426-e83.
2. Ma J, Li Y, Yang X, Liu K, Zhang X, Zuo X, et al. Signaling pathways in vascular function and hypertension: molecular mechanisms and therapeutic interventions. Signal Transduct Target Ther. 2023;8(1):168.
3. Wynne BM, Chiao CW, Webb RC. Vascular Smooth Muscle Cell Signaling Mechanisms for Contraction to Angiotensin II and Endothelin-1. J Am Soc Hypertens. 2009;3(2):84-95.
4. Miller E, Czopek A, Duthie KM, Kirkby NS, van de Putte EE, Christen S, et al. Smooth Muscle Endothelin B Receptors Regulate Blood Pressure but Not Vascular Function or Neointimal Remodeling. Hypertension. 2017;69(2):275-85.
5. Murakoshi N, Miyauchi T, Kakinuma Y, Ohuchi T, Goto K, Yanagisawa M, et al. Vascular endothelin-B receptor system in vivo plays a favorable inhibitory role in vascular remodeling after injury revealed by endothelin-B receptor-knockout mice. Circulation. 2002;106(15):1991-8.
6. Mack CP, Thompson MM, Lawrenz-Smith S, Owens GK. Smooth muscle alpha-actin CArG elements coordinate formation of a smooth muscle cell-selective, serum response factor-containing activation complex. Circ Res. 2000;86(2):221-32.
7. McDonald OG, Wamhoff BR, Hoofnagle MH, Owens GK. Control of SRF binding to CArG box chromatin regulates smooth muscle gene expression in vivo. J Clin Invest. 2006;116(1):36-48.
8. Yoshida T, Sinha S, Dandré F, Wamhoff BR, Hoofnagle MH, Kremer BE, et al. Myocardin is a key regulator of CArG-dependent transcription of multiple smooth muscle marker genes. Circ Res. 2003;92(8):856-64.
9. Parmacek MS. Myocardin-related transcription factors: critical coactivators regulating cardiovascular development and adaptation. Circ Res. 2007;100(5):633-44.
10. Subramanian SV, Polikandriotis JA, Kelm RJ, David JJ, Orosz CG, Strauch AR. Induction of vascular smooth muscle alpha-actin gene transcription in transforming growth factor beta1-activated myofibroblasts mediated by dynamic interplay between the Pur repressor proteins and Sp1/Smad coactivators. Mol Biol Cell. 2004;15(10):4532-43.
11. Qiu P, Ritchie RP, Fu Z, Cao D, Cumming J, Miano JM, et al. Myocardin enhances Smad3-mediated transforming growth factor-beta1 signaling in a CArG box-independent manner: Smad-binding element is an important cis element for SM22alpha transcription in vivo. Circ Res. 2005;97(10):983-91.
12. Deaton RA, Gan Q, Owens GK. Sp1-dependent activation of KLF4 is required for PDGF-BB-induced phenotypic modulation of smooth muscle. Am J Physiol Heart Circ Physiol. 2009;296(4):H1027-37.
13. Mack CP. Signaling mechanisms that regulate smooth muscle cell differentiation. Arterioscler Thromb Vasc Biol. 2011;31(7):1495-505.
14. Regan CP, Adam PJ, Madsen CS, Owens GK. Molecular mechanisms of decreased smooth muscle differentiation marker expression after vascular injury. J Clin Invest. 2000;106(9):1139-47.
15. Shankman LS, Gomez D, Cherepanova OA, Salmon M, Alencar GF, Haskins RM, et al. KLF4-dependent phenotypic modulation of smooth muscle cells has a key role in atherosclerotic plaque pathogenesis. Nat Med. 2015;21(6):628-37.
16. Yoshida T, Gan Q, Owens GK. Kruppel-like factor 4, Elk-1, and histone deacetylases cooperatively suppress smooth muscle cell differentiation markers in response to oxidized phospholipids. Am J Physiol Cell Physiol. 2008;295(5):C1175-82.

17. Perisic Matic L, Rykaczewska U, Razuvaev A, Sabater-Lleal M, Lengquist M, Miller CL, et al. Phenotypic Modulation of Smooth Muscle Cells in Atherosclerosis Is Associated With Downregulation of LMOD1, SYNPO2, PDLIM7, PLN, and SYNM. Arterioscler Thromb Vasc Biol. 2016;36(9):1947-61.
18. Kimball AS, Davis FM, denDekker A, Joshi AD, Schaller MA, Bermick J, et al. The Histone Methyltransferase Setdb2 Modulates Macrophage Phenotype and Uric Acid Production in Diabetic Wound Repair. Immunity. 2019;51(2):258-71.e5.
19. Gallagher KA, Joshi A, Carson WF, Schaller M, Allen R, Mukerjee S, et al. Epigenetic changes in bone marrow progenitor cells influence the inflammatory phenotype and alter wound healing in type 2 diabetes. Diabetes. 2015;64(4):1420-30.
20. Zou M, Mangum KD, Magin JC, Cao HH, Yarboro MT, Shelton EL, et al. Prdm6 drives ductus arteriosus closure by promoting ductus arteriosus smooth muscle cell identity and contractility. JCI Insight. 2023;8(5).
21. Qiu P, Li L. Histone acetylation and recruitment of serum responsive factor and CREB-binding protein onto SM22 promoter during SM22 gene expression. Circ Res. 2002;90(8):858-65.
22. Cao D, Wang Z, Zhang CL, Oh J, Xing W, Li S, et al. Modulation of smooth muscle gene expression by association of histone acetyltransferases and deacetylases with myocardin. Mol Cell Biol. 2005;25(1):364-76.
23. Chakraborty R, Ostriker AC, Xie Y, Dave JM, Gamez-Mendez A, Chatterjee P, et al. Histone Acetyltransferases p300 and CBP Coordinate Distinct Chromatin Remodeling Programs in Vascular Smooth Muscle Plasticity. Circulation. 2022;145(23):1720-37.
24. Liu R, Jin Y, Tang WH, Qin L, Zhang X, Tellides G, et al. Ten-eleven translocation-2 (TET2) is a master regulator of smooth muscle cell plasticity. Circulation. 2013;128(18):2047-57.
25. Findeisen HM, Gizard F, Zhao Y, Qing H, Heywood EB, Jones KL, et al. Epigenetic regulation of vascular smooth muscle cell proliferation and neointima formation by histone deacetylase inhibition. Arterioscler Thromb Vasc Biol. 2011;31(4):851-60.
26. Salmon M, Gomez D, Greene E, Shankman L, Owens GK. Cooperative binding of KLF4, pELK-1, and HDAC2 to a G/C repressor element in the SM22α promoter mediates transcriptional silencing during SMC phenotypic switching in vivo. Circ Res. 2012;111(6):685-96.
27. Liu M, Espinosa-Diez C, Mahan S, Du M, Nguyen AT, Hahn S, et al. H3K4 di-methylation governs smooth muscle lineage identity and promotes vascular homeostasis by restraining plasticity. Dev Cell. 2021;56(19):2765-82.e10.
28. Ehret GB, Munroe PB, Rice KM, Bochud M, Johnson AD, Chasman DI, et al. Genetic variants in novel pathways influence blood pressure and cardiovascular disease risk. Nature. 2011;478(7367):103-9.
29. Giri A, Hellwege JN, Keaton JM, Park J, Qiu C, Warren HR, et al. Trans-ethnic association study of blood pressure determinants in over 750,000 individuals. Nat Genet. 2019;51(1):51-62.
30. Davis FM, Tsoi LC, Melvin WJ, denDekker A, Wasikowski R, Joshi AD, et al. Inhibition of macrophage histone demethylase JMJD3 protects against abdominal aortic aneurysms. J Exp Med. 2021;218(6).
31. Audu CO, Melvin WJ, Joshi AD, Wolf SJ, Moon JY, Davis FM, et al. Macrophage-specific inhibition of the histone demethylase JMJD3 decreases STING and pathologic inflammation in diabetic wound repair. Cell Mol Immunol. 2022;19(11):1251-62.
32. Davis FM, Melvin WJ, Mangum K, Tsoi LC, Joshi AD, Cai Q, et al. The Histone Methyltransferase SETDB2 Modulates Tissue Inhibitors of Metalloproteinase-Matrix Metalloproteinase Activity During Abdominal Aortic Aneurysm Development. Ann Surg. 2023;278(3):426-40.
33. Plotnikov D, Huang Y, Khawaja AP, Foster PJ, Zhu Z, Guggenheim JA, et al. High Blood Pressure and Intraocular Pressure: A Mendelian Randomization Study. Invest Ophthalmol Vis Sci. 2022;63(6):29.

34. Wu Y, Byrne EM, Zheng Z, Kemper KE, Yengo L, Mallett AJ, et al. Genome-wide association study of medication-use and associated disease in the UK Biobank. Nat Commun. 2019;10(1):1891.
35. Kruidenier L, Chung CW, Cheng Z, Liddle J, Che K, Joberty G, et al. A selective jumonji H3K27 demethylase inhibitor modulates the proinflammatory macrophage response. Nature. 2012;488(7411):404-8.
36. Nassar LR, Barber GP, Benet-Pagès A, Casper J, Clawson H, Diekhans M, et al. The UCSC Genome Browser database: 2023 update. Nucleic Acids Res. 2023;51(D1):D1188-D95.
37. Rauluseviciute I, Riudavets-Puig R, Blanc-Mathieu R, Castro-Mondragon JA, Ferenc K, Kumar V, et al. JASPAR 2024: 20th anniversary of the open-access database of transcription factor binding profiles. Nucleic Acids Res. 2023.
38. Hautmann MB, Madsen CS, Owens GK. A transforming growth factor beta (TGFbeta) control element drives TGFbeta-induced stimulation of smooth muscle alpha-actin gene expression in concert with two CArG elements. J Biol Chem. 1997;272(16):10948-56.
39. Luo G, Jamali R, Cao YX, Edvinsson L, Xu CB. Vascular endothelin ET(B) receptor-mediated contraction requires phosphorylation of ERK1/2 proteins. Eur J Pharmacol. 2006;538(1-3):124-31.
40. D'Angelo G, Adam LP. Inhibition of ERK attenuates force development by lowering myosin light chain phosphorylation. Am J Physiol Heart Circ Physiol. 2002;282(2):H602-10.
41. Schiffrin EL. Vascular remodeling in hypertension: mechanisms and treatment. Hypertension. 2012;59(2):367-74.
42. Owens GK, Kumar MS, Wamhoff BR. Molecular regulation of vascular smooth muscle cell differentiation in development and disease. Physiol Rev. 2004;84(3):767-801.
43. Chen QW, Edvinsson L, Xu CB. Role of ERK/MAPK in endothelin receptor signaling in human aortic smooth muscle cells. BMC Cell Biol. 2009;10:52.
44. Das S, Senapati P, Chen Z, Reddy MA, Ganguly R, Lanting L, et al. Regulation of angiotensin II actions by enhancers and super-enhancers in vascular smooth muscle cells. Nat Commun. 2017;8(1):1467.
45. Azahri NS, Di Bartolo BA, Khachigian LM, Kavurma MM. Sp1, acetylated histone-3 and p300 regulate TRAIL transcription: mechanisms of PDGF-BB-mediated VSMC proliferation and migration. J Cell Biochem. 2012;113(8):2597-606.
46. Bai X, Mangum KD, Dee RA, Stouffer GA, Lee CR, Oni-Orisan A, et al. Blood pressure-associated polymorphism controls ARHGAP42 expression via serum response factor DNA binding. J Clin Invest. 2017;127(2):670-80.
47. Padmanabhan S, Dominiczak AF. Genomics of hypertension: the road to precision medicine. Nat Rev Cardiol. 2021;18(4):235-50.
48. Gupta RM, Hadaya J, Trehan A, Zekavat SM, Roselli C, Klarin D, et al. A Genetic Variant Associated with Five Vascular Diseases Is a Distal Regulator of Endothelin-1 Gene Expression. Cell. 2017;170(3):522-33.e15.
49. Yang F, Lai X, Deng L, Liu X, Li J, Zeng S, et al. Association of endothelin-1 gene polymorphisms with the clinical phenotype in primary nephrotic syndrome of children. Life Sci. 2014;118(2):446-50.
50. Adua E. Decoding the mechanism of hypertension through multiomics profiling. J Hum Hypertens. 2023;37(4):253-64.
51. Han S, Uludag MO, Usanmaz SE, Ayaloglu-Butun F, Akcali KC, Demirel-Yilmaz E. Resveratrol affects histone 3 lysine 27 methylation of vessels and blood biomarkers in DOCA salt-induced hypertension. Mol Biol Rep. 2015;42(1):35-42.
52. Krawczyk KK, Skovsted GF, Perisic L, Dreier R, Berg JO, Hedin U, et al. Expression of endothelin type B receptors (EDNRB) on smooth muscle cells is controlled by MKL2, ternary complex factors, and actin dynamics. Am J Physiol Cell Physiol. 2018;315(6):C873-C84.

53. Kimball A, Schaller M, Joshi A, Davis FM, denDekker A, Boniakowski A, et al. Ly6C. Arterioscler Thromb Vasc Biol. 2018;38(5):1102-14.
54. Bolger AM, Lohse M, Usadel B. Trimmomatic: a flexible trimmer for Illumina sequence data. Bioinformatics. 2014;30(15):2114-20.
55. Kim D, Langmead B, Salzberg SL. HISAT: a fast spliced aligner with low memory requirements. Nat Methods. 2015;12(4):357-60.
56. Liao Y, Smyth GK, Shi W. featureCounts: an efficient general purpose program for assigning sequence reads to genomic features. Bioinformatics. 2014;30(7):923-30.
57. Robinson MD, McCarthy DJ, Smyth GK. edgeR: a Bioconductor package for differential expression analysis of digital gene expression data. Bioinformatics. 2010;26(1):139-40.
58. Li B, Tsoi LC, Swindell WR, Gudjonsson JE, Tejasvi T, Johnston A, et al. Transcriptome analysis of psoriasis in a large case-control sample: RNA-seq provides insights into disease mechanisms. J Invest Dermatol. 2014;134(7):1828-38.
59. Dobin A, Davis CA, Schlesinger F, Drenkow J, Zaleski C, Jha S, et al. STAR: ultrafast universal RNA-seq aligner. Bioinformatics. 2013;29(1):15-21.
60. Anders S, Pyl PT, Huber W. HTSeq--a Python framework to work with high-throughput sequencing data. Bioinformatics. 2015;31(2):166-9.
61. Love MI, Huber W, Anders S. Moderated estimation of fold change and dispersion for RNA-seq data with DESeq2. Genome Biol. 2014;15(12):550.
62. Butler A, Hoffman P, Smibert P, Papalexi E, Satija R. Integrating single-cell transcriptomic data across different conditions, technologies, and species. Nat Biotechnol. 2018;36(5):411-20.

Tables and Figures with Legends

Chr	Position	rsID	Effect Allele	Effect Allele Freq	Beta	P-value	Bayes Factor	Posterior Probability
17	7740170	rs62059712	C	0.08	-0.47	1.442e-24	5.2e+19	0.9814
17	7815712	rs79930761	T	0.09	-0.44	1.108e-22	6.4e+17	0.0123
17	7789542	rs7503751	A	0.09	-0.44	2.880e-22	2.6e+17	0.0049

Table 1. Statistical Fine Mapping of GWAS Locus (chr17:7490170-7990170) with 99.9% credible set. Results of Bayes factor fine mapping analysis of a candidate 500kb region, 250kb upstream and downstream of rs62059712.

Homo_sapiens	GTGTTAGAGGTGGCCTGGGAT
Mus_musculus	GTGTTCGAGGTGGCCTGGGAT
Castor_canadensis	GTGTTAGAGGTGGCCTGGGGT
Dipodomys_ordii	GTGTTAAAGGTGGCCTGGGAT
Cricetulus_griseus_picr	GTGTTAGAGGTGGCCTGGGAT
Mesocricetus_auratus	GTGTTAGAGGTGGCCTGGGAT
Microtus_ochrogaster	GTGTTAGAGGTGGCCTGGGAT
Peromyscus_maniculatus_bairdii	GTGTTAGAGGTGGCCTGGGAT
Meriones_unguiculatus	GTGTTAGAGGTGGCCTGGGAT
Mus_spicilegus	GTGTTCGAGGTGGCCTGGGAT
Rattus_norvegicus	GTGTTCTAGGTGGCCTGGGAT
Nannospalax_galili	GTGTTAGAGGTGGCCTGGGAT
Jaculus_jaculus	GTGTTAGAGGTGGCCCGGGGT
Cavia_porcellus	GTGTTAGAGGTGGCCTAGGAT
Chinchilla_lanigera	GTGTTAGAGGTGGCCTAGGAT
Octodon_degus	GTGTTAGAGGTGGCCTAGGAT
Fukomys_damarensis	GTGTTTGAGGTAGCCTAGGAT
Heterocephalus_glaber_female	GTGTTAGAGGTGGCCTAGGAT
Ictidomys_tridecemlineatus	GTGTTAGAGGTGGCCTAGGAT
Urocitellus_parryii	GTGTTAGAGGTGGCCTAGGAT
Spermophilus_dauricus	GTGTTAGAGGTGGCCTAGGAT
Marmota_marmota_marmota	GTGTTAGAGGTGGCCTAGGAT
Sciurus_vulgaris	GTGTTAGAGGTGGCCTAGGAT

Table 2. Comparison of rs62059712 contained within the SP1 binding consensus region across rodent species. Conservation of rs62059712 in humans and across several rodent species was analyzed within Ensembl.

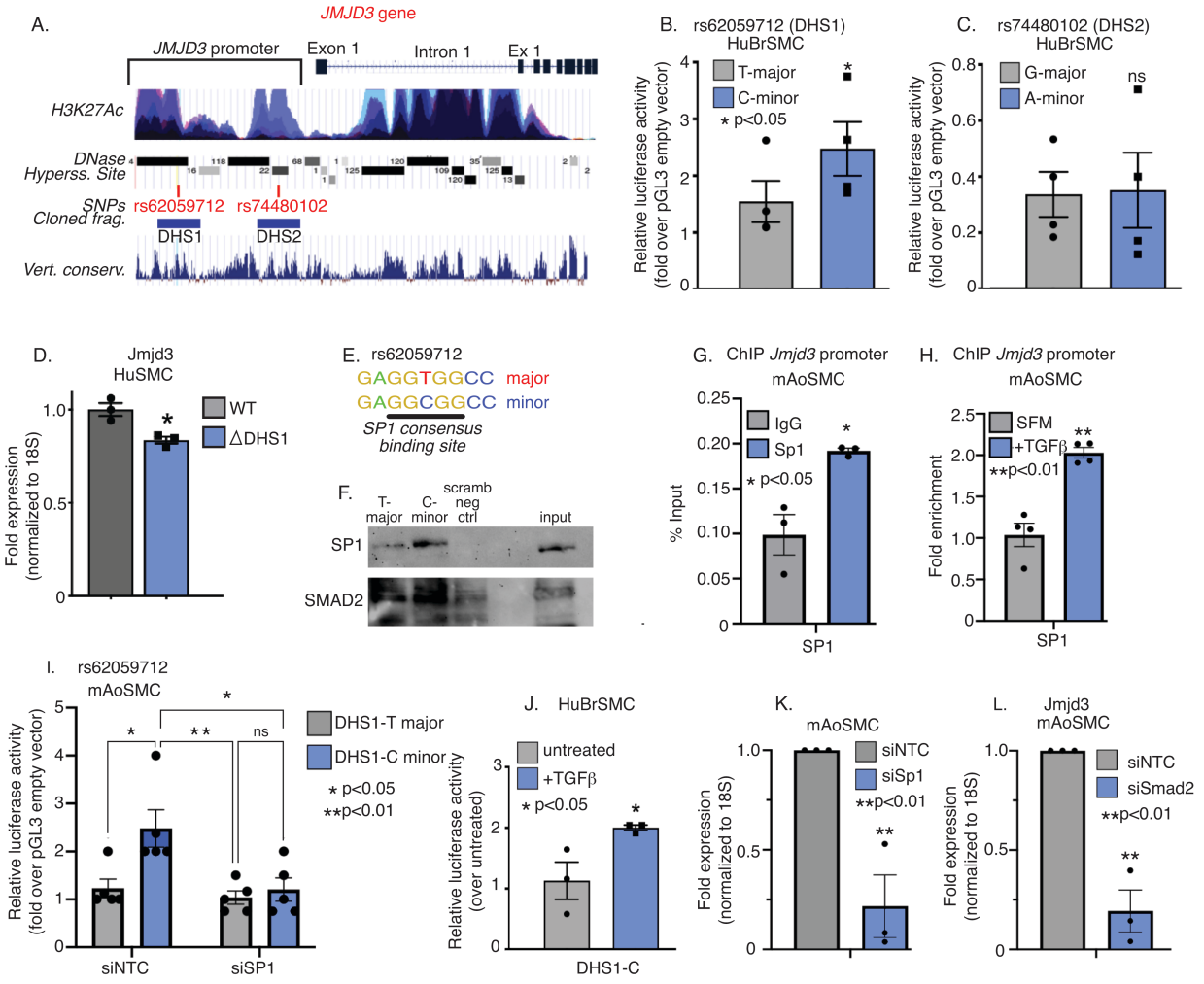

Figure 1. rs62059712 minor C allele increases JMJD3 transcription via enhanced SP1 binding. A) Schematic of the human *JMJD3* gene including gene structure, H3K27Ac, DHS, BP-associated SNPs, cloned fragments for luciferase assays, and vertebrate conservation (UCSC genome browser). B) Luciferase results of DHS1 rs62059712 (T-major vs. C-minor) and C) DHS2 rs74480102 (G-major vs. A-minor) in cultured primary HuBrSMCs. D) qPCR for *JMJD3* in HuSMCs with CRISPR-Cas9-mediated deletion of a 450 bp region encompassing rs62059712 within DHS1 (ΔDHS1) compared with unedited (WT) HuSMCs. E) Sequence of rs62059712 T-major and C-minor sequences with SP1 consensus binding site underlined. F) Western blot for SP1 after affinity purification using T vs. C probes corresponding to rs62059712 SNP region incubated with HuAoSMC nuclear lysate. G) ChIP-qPCR for Sp1 at the *Jmjd3* promoter in

mAoSMCs compared to IgG negative control. H) ChIP-qPCR for Sp1 at the *Jmjd3* promoter in mAoSMCs serum starved or treated with TGFβ. I) Luciferase assays in mAoSMCs treated with siNTC and siSp1 siRNAs then transfected with pGL3-DHS1-T and -C. J) Luciferase assays in HuSMCs transfected with DHS1-C construct and then treated with TGFβ (20 ng/ml). K) qPCR for *Jmjd3* after NTC vs. Sp1 knockdown in mAoSMCs serum starved for 16 hours. Data are presented as mean ± SEM. Results representative of data from SMCs from 4-6 mice per group, n=3 independent experiments. Two-tailed Student's *t* test, *p<0.05, **p<0.01.

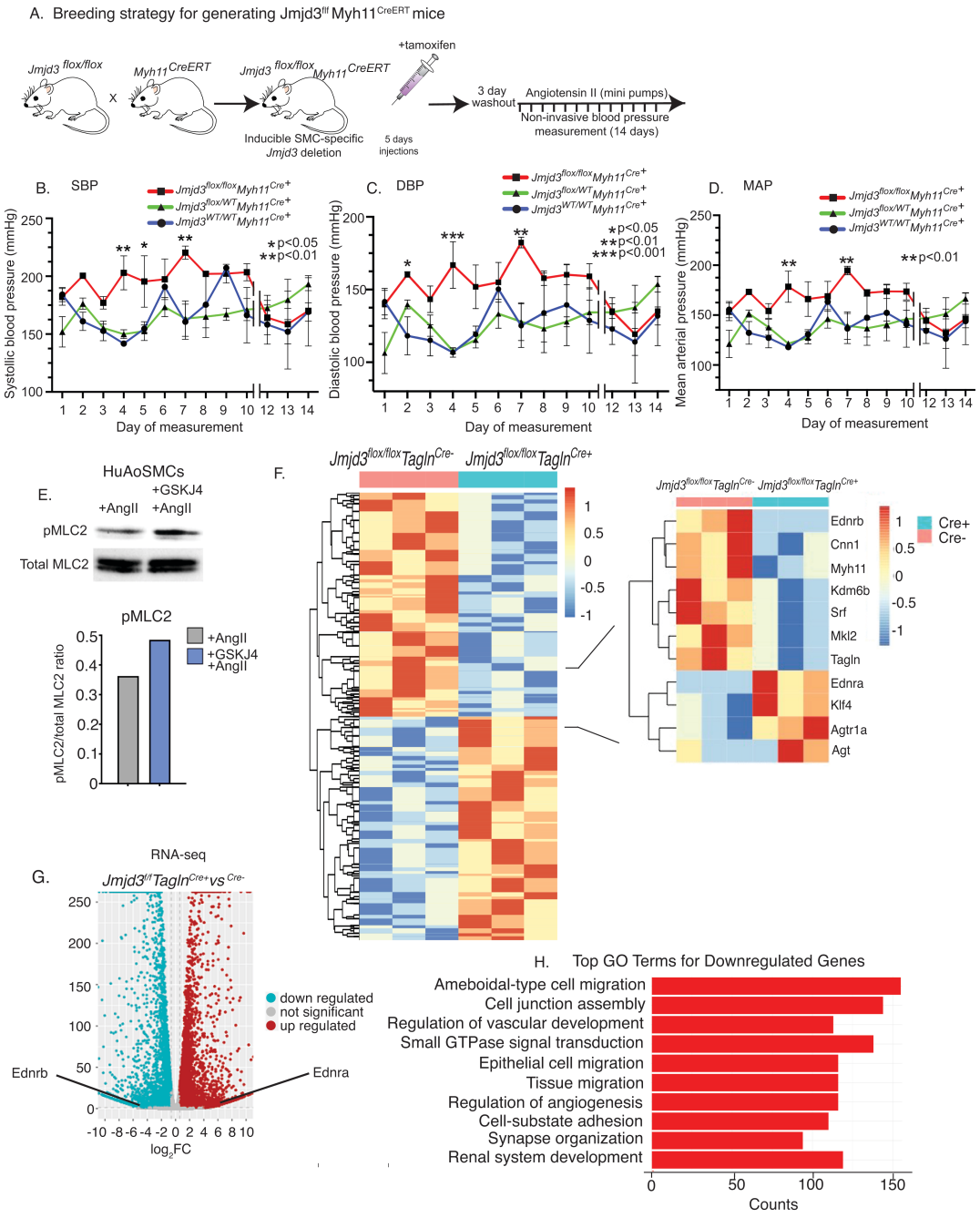

Figure 2. JMJD3 loss in vascular smooth muscle cells results in hypertension. A) Schematic depicting experiment and breeding strategy for generating inducible SMC-specific Jmjd3 knockout *Jmjd3*$^{flox/flox}$*Myh11*^{CreERT} mice. BP obtained by tail cuff for 14 days in WT, heterozygous, and homozygous *Jmjd3*$^{flox/flox}$*Myh11*^{CreERT} mice treated with Angiotensin II via osmotic minipumps. B) Systolic blood pressure (SBP), C) Diastolic blood pressure (DBP), and D) Mean arterial

pressure (MAP) are depicted. N=4-6 mice per genotype/group. E) HuAoSMCs were treated with Angiotensin II (100 nM) or Angiotensin II and GSKJ4 (50 nM) and then analyzed for phospho-myosin light chain 2 (pMLC2) and total MLC2 by western blotting. Blot is representative of n=3 independent experiments with representative densitometry depicted below. F) DEGs obtained from RNA-seq analysis of cultured mAoSMCs isolated from *Jmjd3*$^{flox/flox}$*Tagln*$^{Cre+}$ and *Jmjd3*$^{flox/flox}$*Tagln*$^{Cre-}$ mice with relevant DEGs depicted to right. DEGs depicted met significant threshold of $p<0.05$. Results obtained representative of samples for each genotype submitted in triplicate and obtained from n=6-8 mice per sample. G) Volcano plot for upregulated (red) and downregulated (blue) DEGs with fold-change expression depicted on x-axis. Locations of *Ednrb* and *Ednra* are annotated. H) Bar graph of gene ontology (GO) analysis for top 10 downregulated genes in *Jmjd3*$^{flox/flox}$*Tagln*$^{Cre+}$ SMC from RNA-seq results. Gene pathways listed on y-axis and number of gene counts for each pathway are listed on x-axis. Data are presented as mean ± SEM, n=3 independent experiments for *in vitro* studies. Two-way ANOVA, *$p<0.05$, **$p<0.01$, ***$p<0.001$.

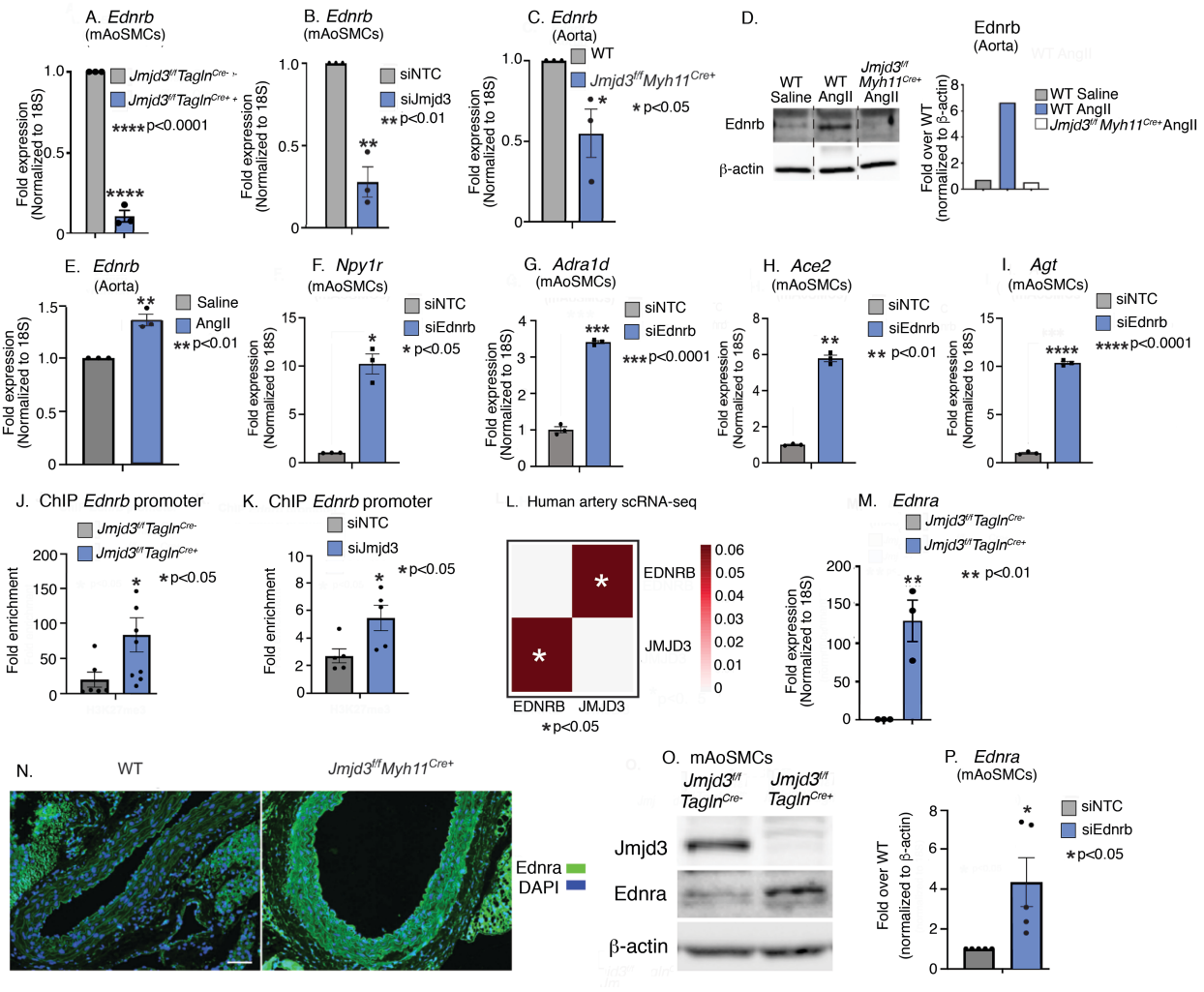

Figure 3. JMJD3 is required for *EDNRB* expression in SMCs and suppresses the hypertensive gene program. A) qPCR of *Ednrb* in SMCs isolated from *Jmjd3*$^{flox/flox}$*Tagln*$^{Cre+}$ and *Jmjd3*$^{flox/flox}$*Tagln*$^{Cre-}$ mice. B) qPCR for *Ednrb* in mAoSMCs treated with siNTC or siJmjd3 siRNA and then serum starved for 16 hours. C) qPCR of *Ednrb* in whole aortic tissue from *Jmjd3*$^{flox/flox}$*Myh11*$^{Cre+}$ and WT mice. D) Representative Western blot and densitometry results for Ednrb in aortas isolated from *Jmjd3*$^{flox/flox}$*Myh11*$^{Cre+}$ and WT mice after 14 days of Angiotensin II or saline infusion. Representative densitometry depicted to right. E) qPCR for *Ednrb* in aortas isolated from WT mice treated with saline or Angiotensin II for 14 days. F) qPCR for *Npy1r, Adra1d* (G), *Ace2* (H), and *Agt* (I) after Ednrb knockdown in mAoSMCs then serum started for 16 hours. J) ChIP-qPCR for H3K27me3 at *Ednrb* promoter in *Jmjd3*$^{flox/flox}$*Tagln*^{Cre} mAoSMCs. K) ChIP-qPCR

for H3K27me3 at the *Ednrb* promoter in mAoSMCs treated with siNTC or siJmjd3 siRNA. L) scRNA-seq data from human femoral arteries showing Pearson correlation between *JMJD3* and *EDNRB* in SMCs, n=4 samples. M) qPCR of *Ednra* in SMCs isolated from $Jmjd3^{flox/flox}Tagln^{Cre}$ mice. N) Representative images of immunofluorescent staining for Ednra in aortas harvested from $Jmjd3^{flox/flox}Myh11^{Cre+}$ and WT mice in (D). Scale bar, 50 um. O) Representative western blotting results for Jmjd3 and Ednra in mAoSMCs from $Jmjd3^{flox/flox}Tagln^{Cre+}$ or $Jmjd3^{flox/flox}Tagln^{Cre-}$ mice. P) qPCR for *Ednra* in mAoSMCs treated with siNTC or siEdnrb siRNA then serum starved for 16 hours. Data are presented as mean ± SEM, n=3 independent experiments, representative of 4-6 mice per group. Two-tailed Student's *t* test, *p<0.05, **p<0.01, ***<0.0001.

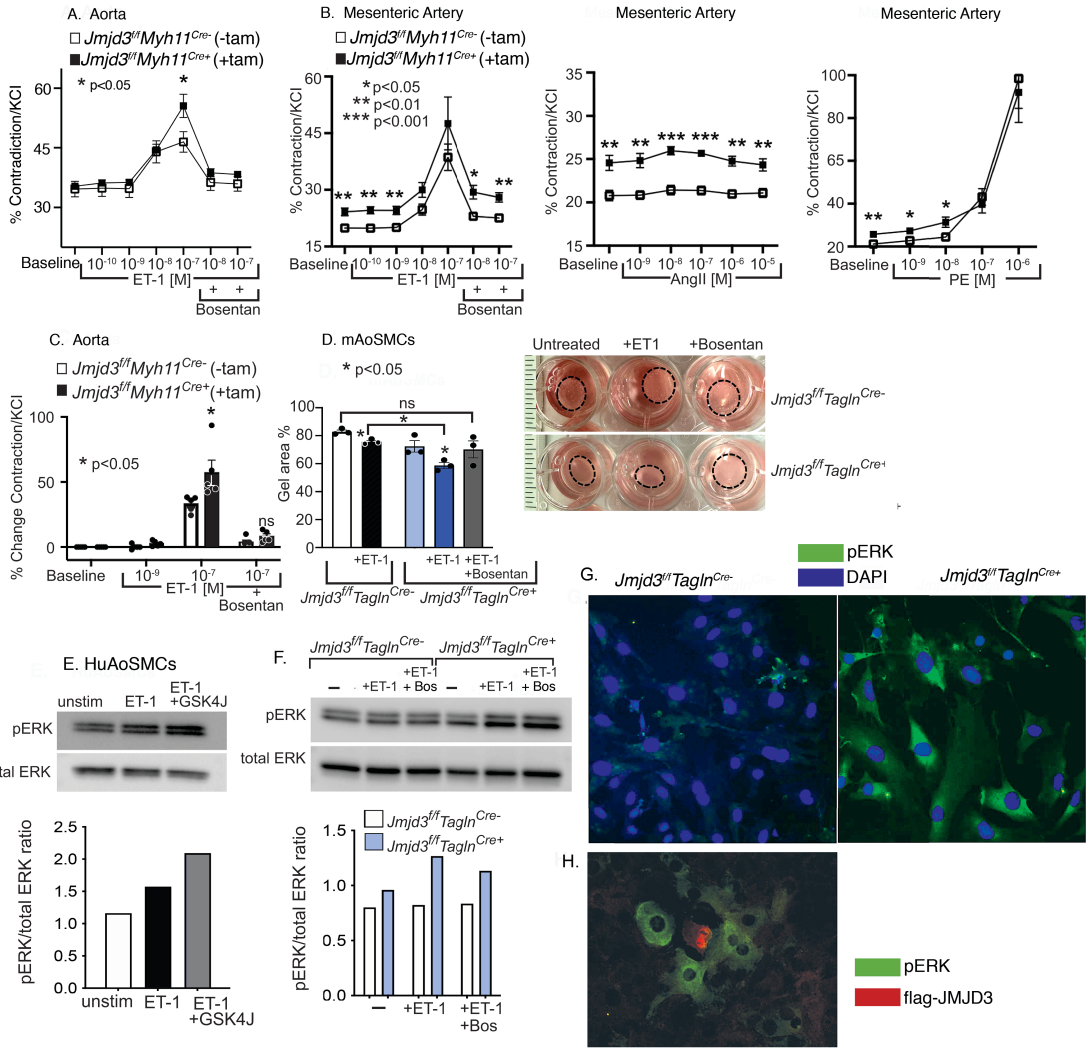

Figure 4. JMJD3 regulates vessel tone via endothelin-ERK signaling in vascular smooth muscle cells. A) Contractility of aortas harvested from *Jmjd3*$^{flox/flox}$*Myh11*$^{Cre+}$ and *Jmjd3*$^{flox/flox}$*Myh11*$^{Cre-}$ mice in response to endothelin-1 (ET-1, 0-10^{-7} M) and bosentan (10^{-8}-10^{-7} M). B) Contractility of mesenteric artery segments harvested from same mice as in (A) in response to increasing concentrations of ET-1 (0-10^{-7} M) and bosentan (10^{-8}-10^{-7} M), Angiotensin II (Ang II, 0-10^{-5} M), or Phenylephrine (PE, 0-10^{-6} M). C) Graph depicting percent change contractility of aortic rings treated with ET-1 (0-10^{-7} M) plus or minus bosentan (10^{-7} M). D) Quantified gel areas containing cultured mAoSMCs from *Jmjd3*$^{flox/flox}$*Tagln*^{Cre} mice. Gels treated with ET-1 (1 uM), ET-1 plus bosentan (10 uM), or bosentan alone. Results depicted as percentage

of initial gel area at 24 hours after seeding. E) Representative western blot of HuAoSMCs unstimulated, treated with ET-1 (1 uM), or ET-1 plus GSKJ4 (50 nM) and then probed for phosphorylated ERK (pERK, top) or total ERK (bottom). Blot with representative densitometry results underneath. F) Representative western blot of *Jmjd3*$^{flox/flox}$*Tagln*$^{Cre+}$ and *Jmjd3*$^{flox/flox}$*Tagln*$^{Cre-}$ control mAoSMCs unstimulated, treated with ET-1 (1 uM), or ET-1 plus bosentan (10 um) and then probed for pERK (top) or total ERK (bottom). Blot with representative densitometry results underneath. G) Representative immunofluorescent staining for pERK in *Jmjd3*$^{flox/flox}$*Tagln*$^{Cre+}$ (right) and *Jmjd3*$^{flox/flox}$*Tagln*$^{Cre-}$ (left) mAoSMCs (up to 4 high powered fields counted per experiment). H) Representative immunofluorescent staining of endogenous pERK in mAoSMCs transfected with Flag-Jmjd3. Data are presented as mean ± SEM, n=3 independent experiments, 6 mice were included in each group for contractility experiments. *In vitro* experiments representative of SMCs from 4-6 mice per group. Two-way ANOVA (A-C) and two-tailed Student's t-test (D). *p<0.05, **p<0.01, ***p<0.001.

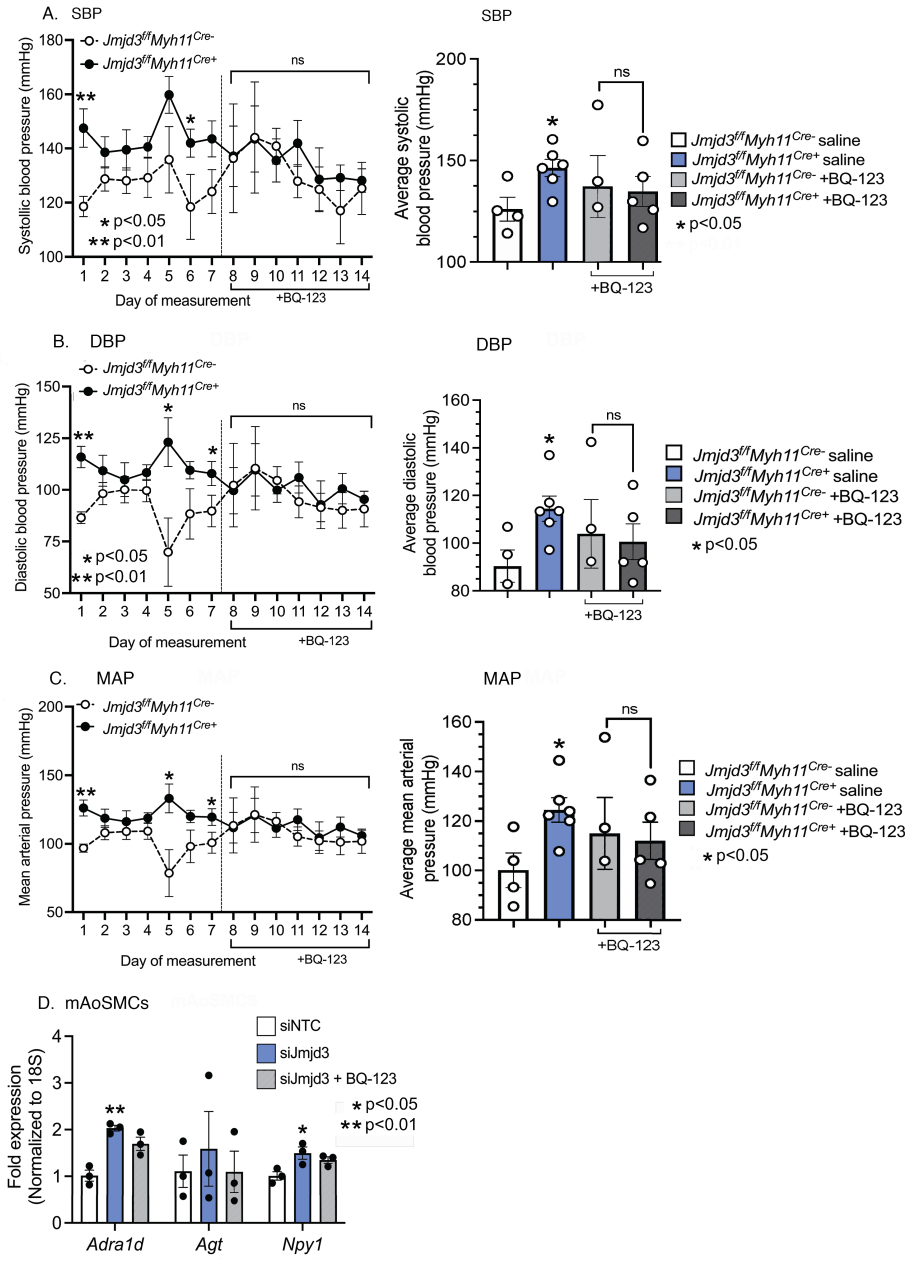

Figure 5. Endothelin receptor A antagonism normalizes blood pressure after JMJD3 deletion in SMCs. BP of *Jmjd3*$^{flox/flox}$*Myh11*$^{Cre+}$ and *Jmjd3*$^{flox/flox}$*Myh11*$^{Cre-}$ mice treated with endothelin receptor A inhibitor, BQ-123 (200 nmol/kg/day), beginning on day 8 of measurements. SBP (A), DBP (B), and MAP (C). Values were also averaged the first 7 days and the final 7 days of the experiment (right of each figure). D) qPCR for *Adra1d, Agt,* and *Npy1* in mAoSMCs transfected with siRNA to Jmjd3 or NTC and then treated with vehicle or BQ-123 (5 uM) for 16

hours. Data are presented as mean ± SEM, n=3 independent experiments. *In vitro* experiments representative of SMCs from 4-6 mice per group. Two-tailed Student's t-test. *p<0.05, **p<0.01.

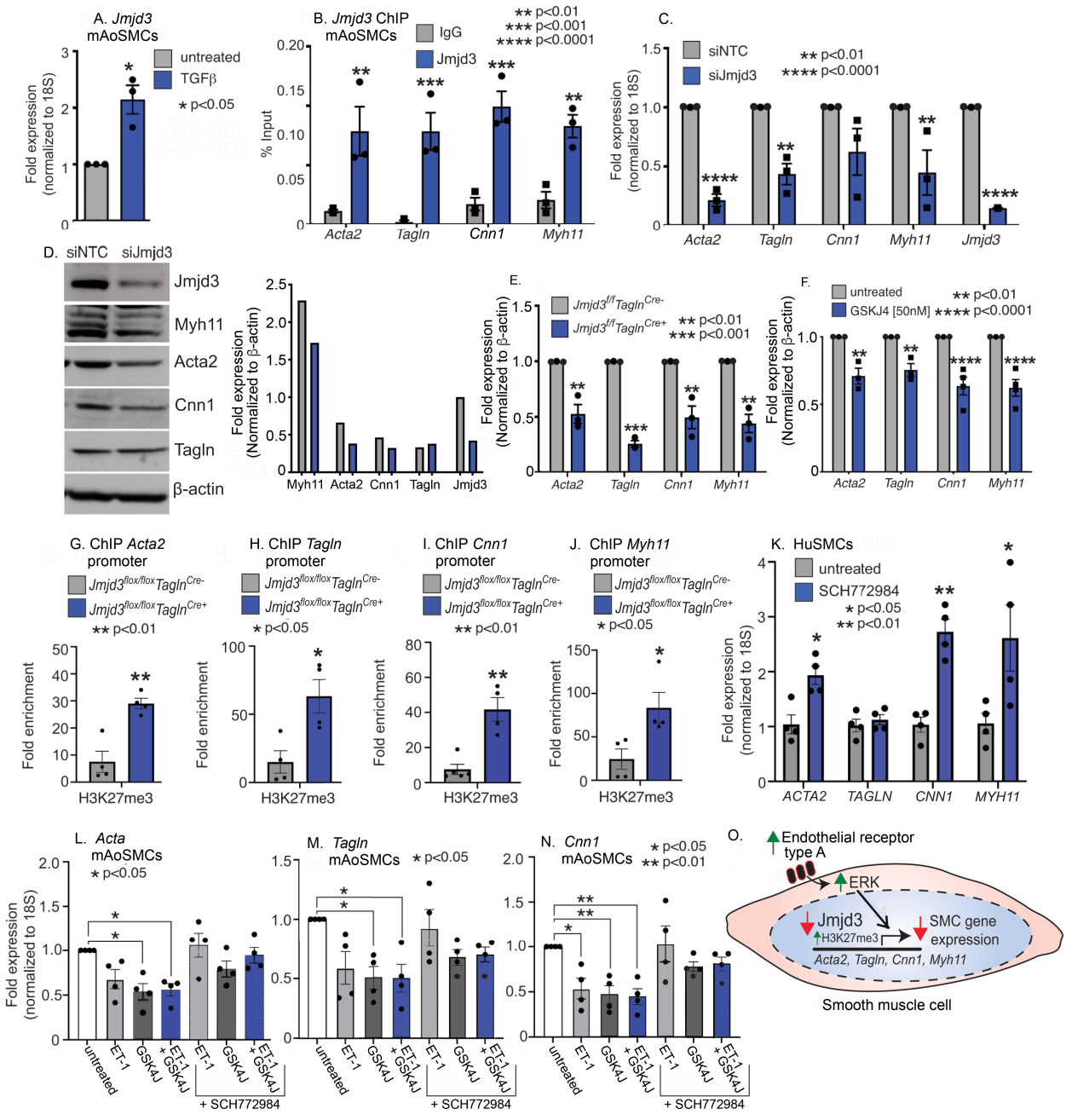

Figure 6. JMJD3 is required for vascular smooth muscle cell differentiation. A) qPCR of *Jmjd3* in mAoSMCs untreated versus treatment with TGFβ (20 ng/ml) for 16 hours. B) ChIP-qPCR showing Jmjd3 enrichment at SMC gene promoters compared to IgG. C) SMC gene expression in mAoSMCs treated with Jmjd3 siRNA or NTC siRNA for 72 hours, serum starved, and then treated with TGFβ (20 ng/ml). D) Representative western blot probed for SMC markers in

mAoSMC lysates treated with Jmjd3 or NTC siRNA. Representative densitometry of blot depicted to right. E) qPCR of smooth muscle genes in *Jmjd3*$^{flox/flox}$*Tagln*^{Cre} mAoSMCs. F) qPCR of *Acta2, Tagln, Cnn1, and Myh11* in mAoSMCs treated with Jmjd3 inhibitor GSKJ4 (50 nM) for 16 hours. G) H3K27me3 ChIP-qPCR at *Acta2*, *Tagln* (H), *Cnn1* (I), *Myh11* (J) promoters in *Jmjd3*$^{flox/flox}$*Tagln*^{Cre} mAoSMCs. K) qPCR for SMC genes in HuSMCs treated with SCH772984 (5 uM) for 16 hours compared to untreated. L) qPCR for *Acta2*, *Tagln* (M), and *Cnn1* (N) in mAoSMCs treated with ET-1 (1 uM), GSK4J (50 nM), ET-1 with GSK4J with or without the ERK inhibitor, SCH772984 (5 uM). O) Illustration depicting effect of JMJD3 loss on SMC gene expression via EDNRA/ERK activation and H3K27me3 at SMC gene promoters. Data are presented as mean ± SEM, n=3 independent experiments. Tissues harvested from 4-6 mice per group. *In vitro* experiments representative of SMCs from 4-6 mice per group. One-way ANOVA (L-N) and two-tailed Student's t-test (A-C, E, F, G-K). *p<0.05, **p<0.01, ***p<0.001, ****p<0.0001.

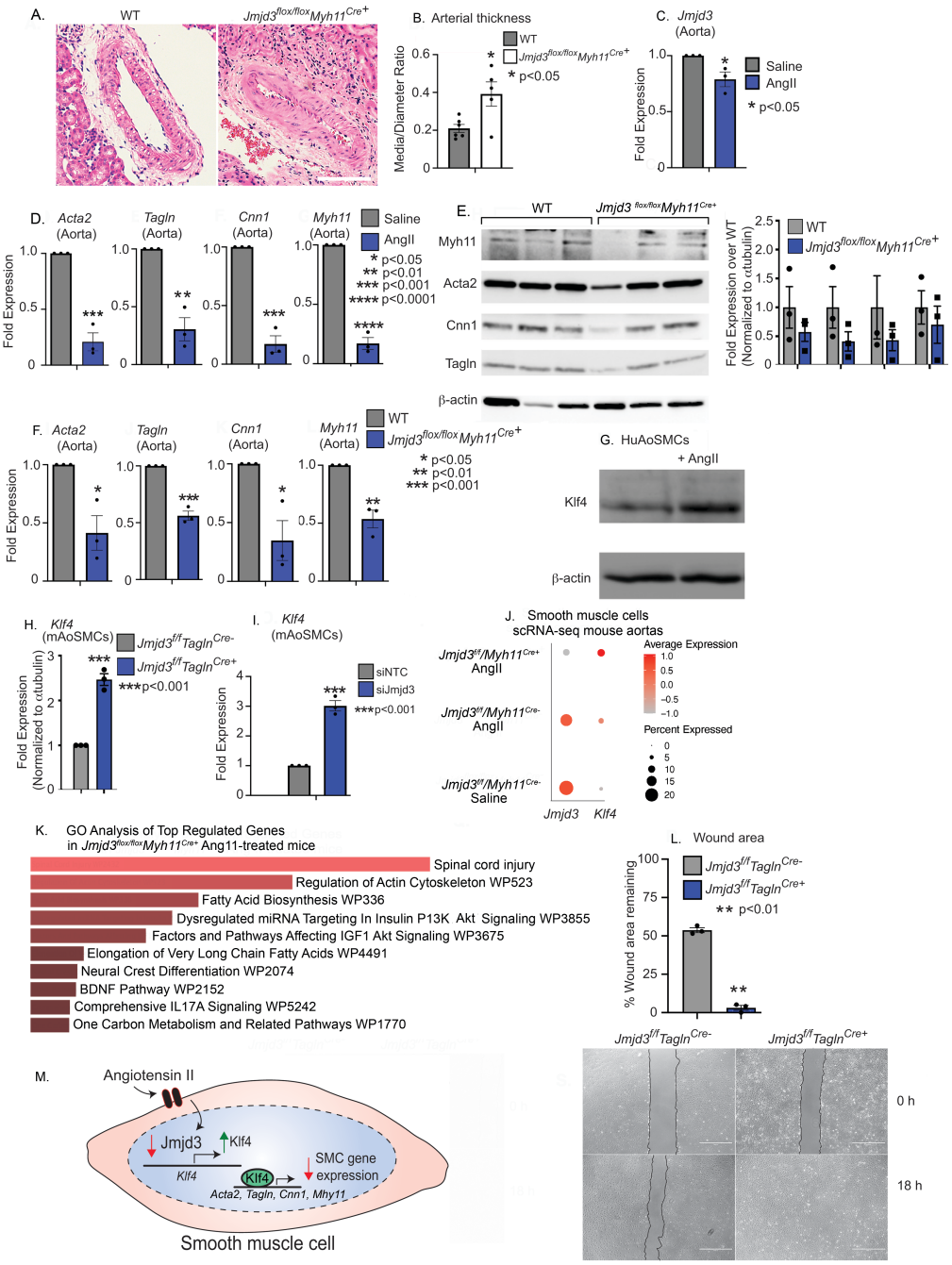

Figure 7. Hypertensive-induced arterial remodeling is regulated by JMJD3. A) H&E staining of kidney sections showing renal arterioles from *Jmjd3*$^{flox/flox}$*Myh11*$^{Cre+}$ and WT mice treated with Angiotensin II (1 ug/kg/min) for 14 days. Scale bar, 100 um. B) Renal arteriole medial wall thickness from (A). C) qPCR for *Jmjd3* in WT aortas from mice treated with 14 days of Angiotensin II or saline. D) qPCR for *Acta2, Tagln, Cnn1, Myh11* in aortas from mice in (C). E) Western blot

for SMC markers from *Jmjd3*$^{flox/flox}$*Myh11*$^{Cre+}$ and WT aortas with densitometry to right. F) qPCR for *Acta2, Tagln*, *Cnn1,* and *Myh11* in aortas from *Jmjd3*$^{flox/flox}$*Myh11*$^{Cre+}$ and WT mice treated with 14 days of Angiotensin II. G) Representative western blot probed for KLF4 in HuAoSMCs serum starved or treated with Angiotensin II for 16 hours. Blot representative of n=3 independent experiments. H) qPCR of *Klf4* expression in *Jmjd3*$^{flox/flox}$*Tagln*^{Cre} mAoSMCs. I) qPCR of *Klf4* in mAoSMCs treated with NTC or siJmjd3 siRNAs and then serum starved for 16 hours. J) Dot plot of *Jmjd3* and *Klf4* generated from scRNA-seq of aortas isolated from *Jmjd3*$^{flox/flox}$*Myh11*^{CreERT} mice treated with saline or Ang II for 14 days (data representative of 2-3 mice per group). K) Histogram of top-most upregulated gene pathways in aortic SMCs from (J). L) Results of scratch assay on *Jmjd3*$^{flox/flox}$*Tagln*^{Cre} mAoSMCs as percent wound area remaining after 18 hours following initial scratch. Representative images at 0 hours and 18 hours after scratch depicted on right. Scale bar, 1 mm. M) Schematic of transcriptional regulation of Angiotensin II-JMJD3-KLF4 axis controlling SMC gene expression. Data presented as mean ± SEM, n=3 independent experiments. Tissues harvested from 4-6 mice per group. *In vitro* experiments representative of SMCs from 4-6 mice per group. Two-tailed Student's t-test. *p<0.05, **p<0.01, ***p<0.001, ****p<0.0001.

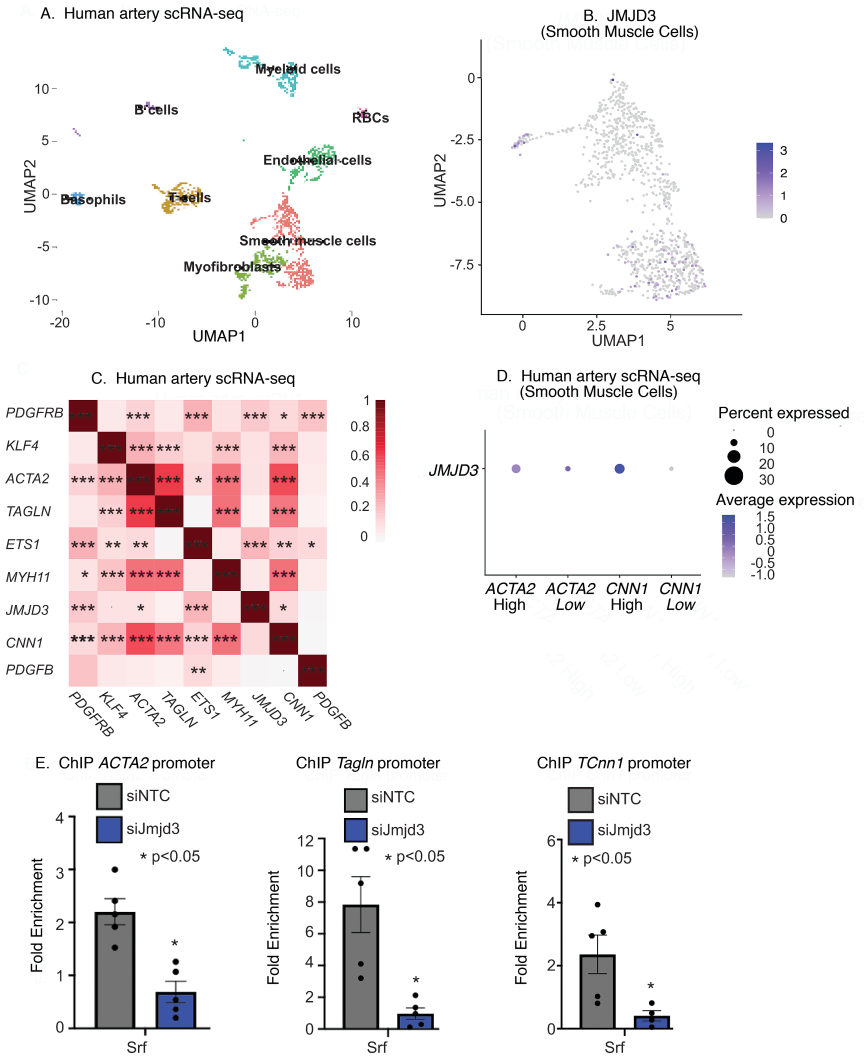

Figure 8. JMJD3 regulates the contractile gene program in SMCs by cooperatively regulating SRF binding to SMC gene promoters. A) UMAP plots of cell populations from scRNA-seq of human femoral arteries (n=4 samples). B) Relative expression of *JMJD3* in SMCs. C) Graph of Pearson correlation of smooth muscle genes from scRNA-seq of human arteries with heat gradient representing strength of association. D) Dot plot of *JMJD3* in human artery SMCs separated by high versus low expression of *ACTA2* and *CNN1*. E) Srf ChIP-qPCR using primers for *Acta2*, *Tagln*, and *Cnn1* promoters in mAoSMCs treated with NTC or siJmjd3 siRNA. Data presented as mean ± SEM, n=3 independent experiments. N=4 human arterial samples.

Experiments representative of SMCs from 4-6 mice per group. Two-tailed Student's t-test and Pearson's correlation coefficient. *p<0.05, **p<0.01, ***p<0.001.